IDŐJÁRÁS

QUARTERLY JOURNAL
OF THE HUNGARIAN METEOROLOGICAL SERVICE

CONTENTS

Special issue: Application of advanced methods used for specific environmental purposes

Guest Editor: Kálmán Kovács

VOL. 127 * NO. 4 * OCTOBER – DECEMBER 2023

IDŐJÁRÁS

Quarterly Journal of the Hungarian Meteorological Service

Editorial Office: Kitaibel P.u. 1, H-1024 Budapest, Hungary
P.O. Box 38, H-1525 Budapest, Hungary
E-mail: journal.idojaras@met.hu

Indexed and abstracted in Science Citation Index Expanded™ and Journal Citation Reports/Science Edition
Covered in the abstract and citation database SCOPUS®
Included in EBSCO's database

Subscription by mail:
IDŐJÁRÁS, P.O. Box 38, H-1525 Budapest, Hungary
E-mail: journal.idojaras@met.hu

Editorial

Special Issue: Application of advanced methods for specific environmental purposes

"At the beginning of the third millennium, the extensive variability of weather has become the most significant risk factor for a number of social-economic areas. This can be particularly seen in the state of the environment and in agriculture, which makes the research of these impacts a priority task. Reasonably, fast advancing scientific areas as space science and information technology play major roles in these researches." A special compilation series of the Quarterly Journal of the Hungarian Meteorological Service was launched with these words in 2010.

This volume is the fifth in this series. The past years clearly supported what was written in the editorial introduction of the first special issue. Moreover, in addition to the state of the environment and agriculture, it certainly seemed justified to include other thematic areas, such as transport and the state of rivers, among the research areas examined in the series. For similar reasons, the range of publishing university and institutional research groups has also widened/expanded over the years.

In order to better understand and evaluate the recent complex environmental changes, advanced investigation methods and technologies are being developed and applied worldwide. They are focusing on almost all key aspects of challenges, including our atmosperic environment and its related natural systems like water, soil, and vegetation. Five papers aiming at some of these goals are presented in this specific issue prepared in close cooperation between natural scientists and engineers.

The first paper of this volume is also a good example of the necessity and justification of expanding the research topic and the circle of authors. The joint work of the author team (*Birinyi et al.*), as a result of the cooperation of several universities and institutions, presents a comprehensive study method of the environmental risk of climate change, which is not only very remarkable in its approach to the topic, but also in its results. The paper deals with the contribution of data-driven methods to risk reduction and climate change adaptation in Hungary and beyond. The severe drought damage that occurred in 2022 urged a thoughtful and long-term concept to tackle and mitigate the effects of similar events. To develop this concept, in addition to taking stock of scientific results so far, it is crucial to establish the basis for mutually supportive cooperation between the sectors concerned, including agriculture, water management, and nature conservation. The continuous deterioration of the landscape's water retention and

evapotranspiration capacity is associated with weakening the climate regulating function and the degradation of agricultural production conditions. Accordingly, the task is not to find new resources and interventions ensuring the continuation of current landscape use; the real goal is to find the landscape use (farming methods and water use) that will ensure sustainable human livelihoods and environmental conditions.

The second paper (*Fridvalszky et al.*) evaluates specific dehazing techniques on artificial and satellite land surface images. Many image-based recognition tasks are highly susceptible to different types of natural phenomena like foggy weather, snow, or rain. The participating media will likely obscure important details necessary for these algorithms to work correctly. Still, these aspects could be recovered in certain situations with prior information about the underlying light interactions. This could be done with certain heuristics or with the nowadays popular deep-learning-based methods. The results of two approaches to remove or scale down the effects of foggy weather are reviewed and compared in this paper.

The third paper (*Szántó* and *Vajta*) deals with one of the special traffic safety effects of the weather. The theme is not new in this series. The first article was published by the editor together with Pál Vécsei in 2014, which presented a detailed statistical analysis of domestic road accidents involving personal injury and the relevant meteorological conditions for the period 1990–2010 in Hungary. In that article, a crowdsourcing-based methodology was presented, supported by a database, which is assembled using data that is far more heterogeneous with regard to acquisition frequency and quality, than those available previously. With their method, driver assistance systems can be created that could indirectly reduce the occurrence of accidents by warning the driver in a given situation. The present paper deals with certain types of medical meteorological phenomenon-transitions that can have a significant deteriorating effect on road safety conditions. Hence, a system that is capable of warning road users of the potential occurence of such conversions can prove to be utterly useful. Vehicles on different levels of automation (i.e., ones equipped with Driver Assistance Systems – DAS) can use this information to adjust their parameters and become more cautious or warn the drivers to be more careful while driving. The developed machine learning model was trained on a dataset covering 10 years of meteorological data in Hungary, and it shows promising results for further development and patent preparation.

The fourth paper (*Kugler* and *Horváth*) presents a comparison of river streamflow measurement from optical and passive microwave radiometry (PMR). The hydrological cycle can be studied both from ground and satellite measurements on a global scale. Yet a comprehensive overview is challenging to establish given the spatial and temporal limitations related to various Earth observation satellite sensors or to maintenance of in-situ gauges. This study aims at comparing the methodology of PMR to optical river gauge measurements based on the assumption, that at selected locations along the river channel, increase in

streamflow is related to increase in the floodplain water surface inundation. Comparison showed a significant obstacle of cloud cover over tropical regions, where PMR has the potential to measure river streamflow. Yet over regions with less clouds, both optical and PMR can be good alternatives to in-situ streamflow ground measurements.

In our country, the cultivation of corn seeds is a priority agricultural area, so the production of the high-quality hybrids required for this is a strategic research topic. In our series, papers on various results are continuously published. The first article of the series (in 2010) dealt with proving that the rate of development of hybrids can be predicted based on knowledge of satellite images and relevant meteorological data. In this volume, the fifth paper (*Gombos et al*.) focuses on the agricultural activity of Debrecen area in Hungary, providing a statistical evaluation of the impact of climate change on maize production during the past 50 years.

The papers published in this volume reflect well the methodological development that has taken place in the field of analysis in recent years, which can be experienced in the application of classical analytical and probabilistic procedures, and especially deep learning and artificial intelligence-based solutions as well. The editor would like to thank the the support of the EU tender project BME_2021-1.2.1-EIT-KIC-2021-00006 and the corresponding domestic project BME_2021-1.2.1-EIT-KIC.

Kálmán Kovács
Guest Editor

DOI:10.28974/idojaras.2023.4.1

IDŐJÁRÁS

Quarterly Journal of the Hungarian Meteorological Service
Vol. 127, No. 4, October – December, 2023, pp. 421–446

Contribution of data-driven methods to risk reduction and climate change adaptation in Hungary and beyond

Edina Birinyi[1,2,*], **Boglárka O. Lakatos**[3,4], **Márta Belényesi**[1], **Dániel Kristóf**[1], **Zsolt Hetesi**[5], **László Mrekva**[5], and **Gábor Mikus**[6]

[1]*Lechner Knowledge Centre, Remote Sensing Division*
Earth Observation Department

[2]*Eötvös Loránd University, Doctoral School of Earth Sciences*

[3]*General Directorate of Water Management, International Department*

[4]*University of Public Service, Faculty of Water Sciences,*
Department of Water and Environmental Policy

[5]*University of Public Service, Faculty of Water Sciences,*
Department of Water and Environmental Security

[6]*Lechner Knowledge Center, Remote Sensing Division*
Budapest, Hungary

**Corresponding author E-mail: edina.birinyi@lechnerkozpont.hu*

Abstract— Among a series of tangible phenomena related to climate change and ecosystem degradation, the severe drought damage that occurred in 2022 urges in particular a thoughtful and long-term concept to tackle and mitigate the effects of similar events. To develop this concept, in addition to taking stock of scientific results so far, it is crucial to establish the basis for mutually supportive cooperation between the sectors concerned, including agriculture, water management, and nature conservation.

As confirmed by scientific knowledge, the continuous deterioration of the landscape's water retention and evapotranspiration capacity is associated with weakening the climate regulating function and the degradation of agricultural production conditions. Accordingly, the task is not to find new resources and interventions ensuring the continuation of current landscape use; the real goal is to find the landscape use (farming methods and water use) that will ensure sustainable human livelihoods and environmental conditions.

All the tools and knowledge are available for the first steps and subsequent ongoing monitoring and refinement of a precautionary and prevention-based approach to support all levels of ecosystem services. With continuous professional dialogue and implementation of established and new methods, several goals can be achieved simultaneously, such as the integration of economic trends into the approach, the revitalization of Hungarian landscape culture, and hence the preservation of the rural workforce.

Key-words: drought, inland excess water, water conservation/retention, prevention-based approach, data-based decision making, remote sensing, Hungary

1. Introduction

Due to the accelerated hydrological cycle and the overuse of the landscape, drought, water scarcity, flash flood, and flood events occur in the same area and more frequently than they used to ("water surplus-water scarcity paradox" – *Kozma et al.*, 2022). According to data from the Hungarian Central Statistical Office (KSH), over the past 10 years, drought has affected more than 70% of the country's territory many times; meanwhile, during wet years of the same period, up to 10–15% of regularly cultivated arable land (> 4 million hectares) was periodically flooded (*KSH*, 2022a,b). The areas affected by both phenomena overlap to a significant extent.

According to the latest data registered in the Agricultural Risk Management System (MKR), extreme water scarcity and heat wave events in the summer of 2022 are among the largest ever observed, and had a very significant impact on agricultural production and natural ecosystems, with more than 1.4 million hectares of arable land affected by drought damage (*MKR*, 2022).

Meanwhile, climate models also show a significant increase in the frequency and probability of extreme events in the Carpathian Basin (*Kis et al.*, 2017; *Torma et al.*, 2020). This situation calls for a well-founded long-term concept, in which it is crucial to establish and strengthen the mutually supportive functioning of sectors concerned, including agriculture, water management, and nature conservation. Further prerequisites are that the concept should build on (i) existing scientific results of climate change and drought research, (ii) data and indicators (statistics) for monitoring drought impacts, and (iii) modern technologies, in particular remote sensing, which can be applied not only for monitoring drought impacts but also for their prediction to some extent. However, the practical implementation of this long-term concept will only be successful if the specific characteristics of areas in question, i.e., local conditions and their effects (landscape history, soil conditions, agrotechnology, etc.) are all considered. In a number of areas, the consequences of land use unsuitable for local landscape conditions cause problems, such as the frequent recurrence of flooding in former flood plains after the regulation of rivers.

Development of monitoring networks in combination with mindful landscape management could contribute to mitigating impacts of extreme events in several ways. Reducing both risks and effects of those implies changes in land use practice to retain water mostly in its original functioning area. Water should be considered the most significant part of the land. The current practice of draining out water during spring floods in the basin is only viable in years of steady water supply, whereas in years with extremely dry spring and summer, the aim should be to maintain high spring yields. Water-focused land use system could provide the "buffer zone":

- for water retention to reduce the upcoming drought effect, or
- to stock water for supporting evapotranspiration, irrigation, and local reduction of temperature, and
- to provide habitat and support at all levels in ecosystem cascades.

Adaptation to extreme weather events in the Carpathian Basin ultimately requires the implementation of circularity among a number of factors such as precipitation, soil conditions, vegetation, new types of crop production, water, nutrients, and (evapo-)transpiration. With the support and extended use of remote sensing data, we are, for instance, able to assess topsoil conditions and infer the available, cost-effective methods to improve soil conditions and health. The purpose of the article is to raise attention to data-driven methods that could take into account certain aspects listed above and contribute to drought-risk reduction and climate change adaptation.

2. Important historical background

2.1. Water management interventions in the Carpathian Basin

In the Carpathian Basin, the Sarmatians already carried out large-scale interventions that had an impact on the hydrographic conditions (e.g., Csörsz ditch), and the Romans also invested in, among other things, ensuring the navigability of rivers. Later, the water management system of the Árpád age, the spread of water mills, crop farming, deforestation under Turkish rule, flooding for military defense purposes, etc., all contributed to the continuous transformation of the hydrographic conditions and the expansion of the bog and marsh world (*Horváth*, 2018).

However, the development of agriculture, the spread of large-scale farming, and the rapidly increasing demand for agricultural crops (mainly grain) have led to more and more water management initiatives in order to increase production areas. In the meantime, commercial shipping also gained more and more space with the appearance of steamships, as well as the reduction of damage caused by floods and the rise of riverbeds caused by sediment deposition. In addition to preventing ice jams, the effective removal of ice dams became an important goal - the latter primarily on the Danube.

In the 19th century, the basic purpose of the regulatory works that began with great force was to help excess waters drain faster, to make water-logged and water-covered areas suitable for arable cultivation by draining them, and to ensure the navigability of our large rivers.

According to *Babinszki* (2017): "Before the river regulations, 13.7 percent (38,771 square kilometers) of historical Hungary was a floodplain, of which 36,700 square kilometers were exempted from flooding. The original floodplain of our country was 22,000 square kilometers, of which the tidal area under the

control of our rivers is only 1,500 square kilometers. By the beginning of the 20th century, bends were cut in 18 places on the river Danube, shortening the river by 123 kilometers. The enormous change in natural geography is even more evident in the data of the Tisza watershed: the 112 crossings of the river Tisza reduced the length of the river by 453 kilometers, and the 248 bends of the rivers Körösök caused a shortening of 546 kilometers".

Thanks to the dam system, which was built as part of the river regulation and got later expanded and gradually heightened, the proportion of areas that could be brought under agricultural production increased, and the settlements in the exempted areas also expanded intensively.

Agricultural production in the landscape, transformed to a great extent due to changed conditions, has thus become more and more intensive, but at the same time has been struggling to this day with numerous negative phenomena partly caused by intensification and land use incompatible with the original landscape conditions. This also includes inland wetlands, whose potential territorial extent shows the pattern of hydrographic conditions before the regulations (*Babinszki*, 2017) (*Fig. 1*).

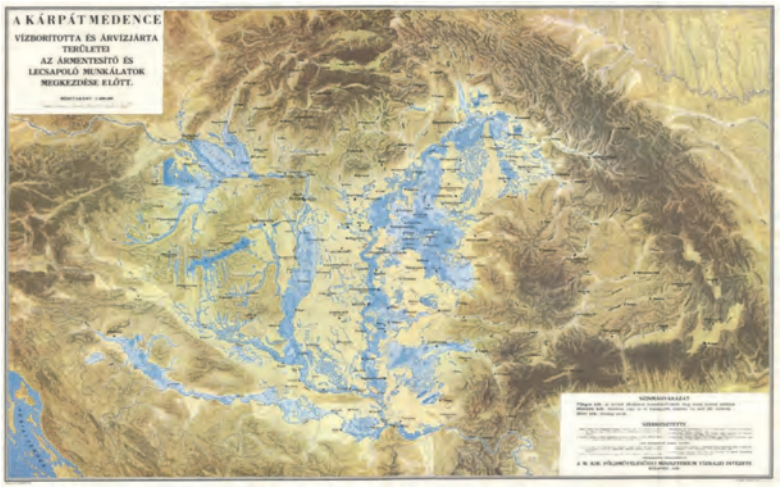

Fig. 1. Water-covered and flood-prone areas of the Carpathian Basin before the start of the relief and drainage works. *Source:* MBFSZ, 2023.

By comparing the maps of the first (1763–1787) and the third (1869–1887) military surveys *(Fig. 2*), some waves of regulatory work can be easily traced. The map sections below show the effects of cutting through the river bend on the example of Tisza River.

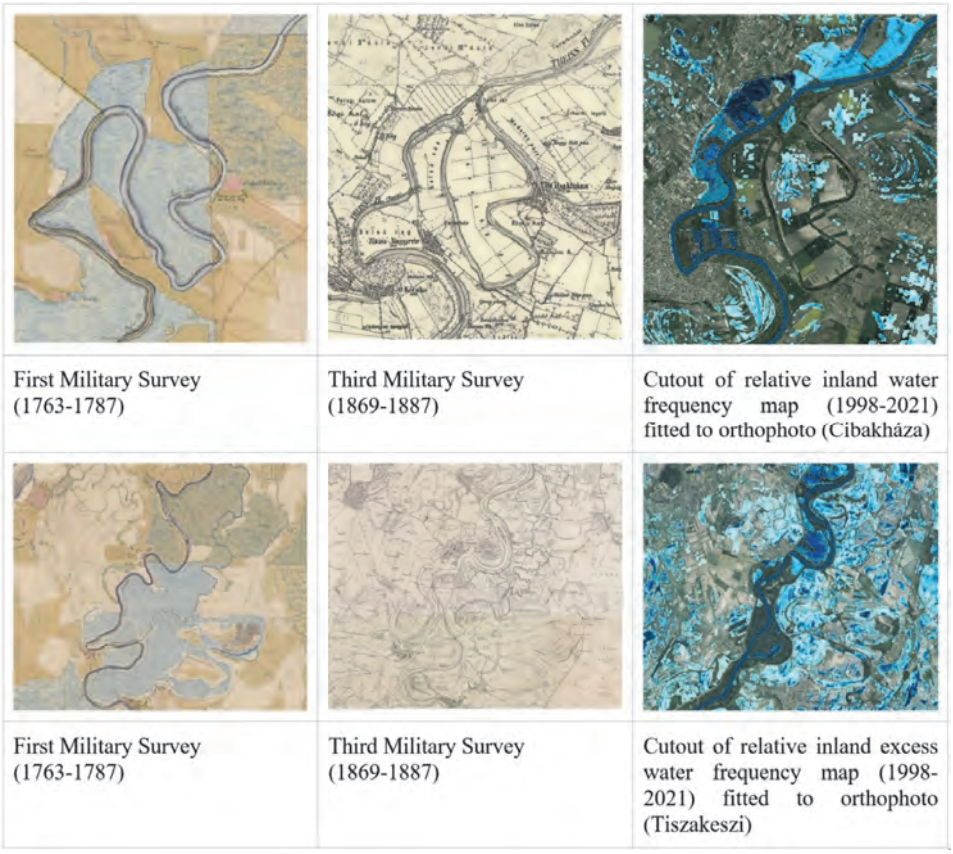

Fig. 2. Comparison of the first and third military surveys, and the relative inland water frequency map sections on examples along the river Tisza. Darker shades of blue represent more frequent inundation. *Source:* Arcanum Adatbázis Kiadó, 2023; LTK, 2023.

2.2. The original landscape-friendly water management

Flood is a natural phenomenon (*Kiedrzyńska et al.,* 2015), it is necessary both for nature as a whole and for farming as well. Groundwater resources along the river can be recharged during floods, which is also necessary for the climate-regulating activities of the forests and groves near the water (*Makarieva et al*., 2005). The floodplains and endemic forests along watercourses are important elements of the natural water system. Their role is essential in balancing the flow of water, preventing flood and drought disasters, and preserving and

utilizing incoming water (*Pálfai et al.,* 2000; *Balogh*, 2001;). Under the influence of the geological structure, the morphological pattern and the natural vegetation cover, the surface and subsurface water cycle sections, the natural systems of the flat and mountainous areas of the Carpathian Basin are connected in a unique way into a cooperative water balance system. Therefore, it can be stated that mountain and lowland forests are the most important governors and preservers of waters of the basin.

The key elements of the outlined system are the floodplains of large extent and the equalizing and life-giving role of excess water management. This ensured the exceptionally good ecological features of the (inner) areas of the Carpathian Basin throughout history. Livelihood activities in floodplains were based on the active cooperation of watercourses, ecosystems, and communities. "Production" adjusted to the conditions of nature not only "withstood" the floods, but the spreading of excess water with human participation - keeping it in motion, and thereby preserving it at the landscape level, ensured the basis of livelihood, such as, for instance, traditional fishing on the Tisza, fruit growing, reed farming, livestock, and medicinal herb collection. Nowadays, the wide range of (eco)tourism opportunities can also be classified here (*Molnár*, 2005; *Kozma et al*., 2022).

3. Connection of soil and water

3.1. Distribution and intensity of precipitation

In Hungary, increasing amounts of precipitation tend to occur outside the vegetation period; hence, to make water available for the vegetation at the right time, it has to be retained and retention capacity of the soil should be increased. Additionally, soil cannot absorb the significant amount of precipitation of increased intensity; therefore, this requires further preparation. We will examine both problems in more detail:

- Changing distribution of precipitation: Currently, a larger part of the annual precipitation in Hungary falls in the summer semester rather than in the winter one. Nevertheless, climate change models predict increasing amounts of winter precipitation (predominantly in the form of rain instead of snow), and decreasing amounts can be expected in summer. This has a negative effect on agricultural crops that still require rainfall during summer because of their longer growing period (e.g., corn, soybeans, or melons). During this period, they would need more water than the amount available from rainfall.
- Increased precipitation intensity and spatial variability: The chance of sudden rains and intense precipitation increases, i.e., the usual amount of precipitation can fall in a shorter time, and its quantity can vary to a large

extent within distances as small as a few hundred meters. The experience of the past years shows that the amount of precipitation during a specific rain event can exceed the usual amount for an entire month or even longer period, especially during thunderstorms.

3.2. Soil, fertility, tillage

During plowing, the topsoil (often containing organic material residues) and the subsoil in contact with the air change places, due to the rotating effect of the plow. However, the decomposition of organic matter is not complete. According to the latest research, the reason for this is that plowing significantly reduces the number of soil-dwelling microbes and specially fungi, while the role of these organisms is crucial in breaking down dead organic matter that forms on top of the soil, and turning it into humus (*De Vries et al.*, 2006).

All over the world, the organic matter content of soils decreases as a result of cultivation. Due to this phenomenon, estimates show that a total of 65-90 x 10^9 metric tons of organic carbon entered the Earth's atmosphere from soils. It is generally true that a 1% excess of organic matter in the soil accounts to 16 tons of organic carbon bound, and this means that an average of 45–65 tons per hectare of carbon disappeared from the Earth's soils. On 1.5 billion hectares of agricultural land, i.e., the organic matter content has decreased by 4% on average. At the end of the 1800s, organic matter content of around 10% could still be measured in the agricultural areas of Hungary; today, it is between 1 and 3% in most areas.

Furthermore, during plowing, the plow pan effect develops in the depth of the plow, i.e., the weight of the plow heads creates a hard, compacted layer during plowing, which the roots cannot break through and is highly impermeable to water. In practice, this means that the upper 25–35 cm of dusty, structureless soil layer must absorb and retain the incoming precipitation.

In addition to the formation of the plow pan layer, however, the structure-destroying effect of tillage has other consequences, as (*Dobos*, 2022a) and his colleagues draw attention to. As the crumbly structure of the soil is lost, its healthy pore system is transformed and degraded. In addition to degrading the healthy water-air ratio, the narrow pores are easily clogged, and the water absorption and retention capacity is drastically reduced. After rain, the soil becomes muddy, a significant part of the water flows on the surface instead of infiltrating, or stalling, forming inland excess water. Later on, the same surface dries out and hardens: "on a hot day, it behaves like concrete in the middle of a big city: it sheds heat from itself, drying out its surroundings, increasing the heat and drought" (*Dobos*, 2022b).

4. State of art of water resource management, affected sectors

4.1. Water management

In Hungary, water management is currently determined by the River Basin Management Plan (VGT) (*OVF*, 2022), which is reviewed every six years based on the Water Framework Directive 2000/60/EC 2000. The first modernized, revised version of VGT1, VGT2, and then VGT3 in 2021, summarizes the loads, condition assessment of our waters, and the progress necessary to achieve good conditions. Based on this, the environmental objectives and action programs for the period between 2021–2027 are determined. In addition, the document "Significant Water Management Issues" (*OVF*, 2019) focuses on the hydrological consequences of drought and climate change, in addition to the quantitative and qualitative issues of surface water, the effect of dams, pollution, and drinking water bases.

Our vulnerability to climate change can be assessed on the basis of the quantity and renewal potential of groundwater resources. The domestic situation is presented on the VGT 3rd Strategic Environmental Assessment (SKV) map and the explanation below (*Fig. 3*).

"In Hungary, due to the effects of climate change, the importance of the fight against extremes in water management is increasing. Without human intervention (passive adaptation), the maintenance of today's water-ecological economic-social conditions cannot be ensured in the future!" (*OVF*, 2022).

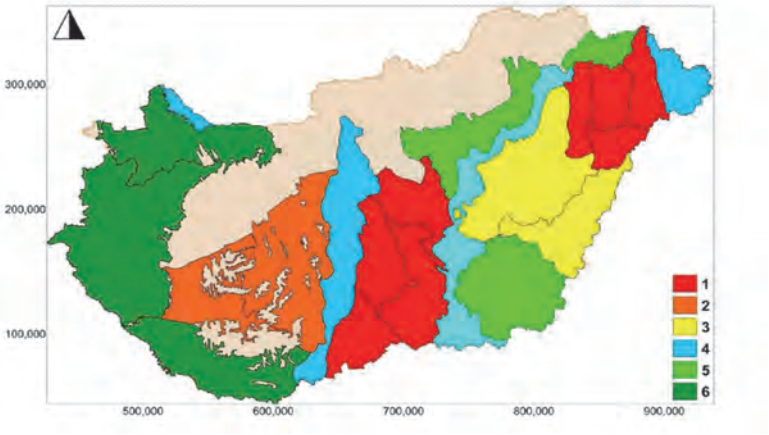

Fig. 3. The threat of groundwater resources due to climate change in the small villages of our country. *Source:* VIZITERV Environ Kft.

The goals set out in the Strategic Environmental Assessment are to create an integrated water management framework based on measurements, so that water damage prevention and water resource management activities can entirely fulfill their role by maintaining or improving ecosystem services (*OVF*, 2021). Water management strategies, action plans, and the proposals for adapting to the effects of climate change – including measures aiming natural water retention and adaption to climate change – are defined in the River Basin Management Plan Hungary 2021 (*OVF*, 2022).

4.2. Agriculture

The extreme water scarcity and heatwave of 2022 have had a significant impact on agricultural production and natural ecosystems. In Hungary, more than 1.4 million hectares of arable land were affected by drought damage (*MKR*, 2022*)*, and it was reflected in the number of agricultural damage claims in 2022 (*Fig. 4*).

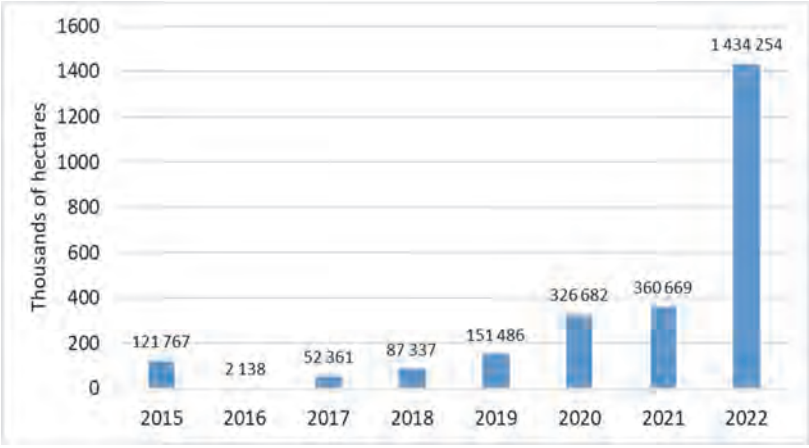

Fig. 4. The total area of drought-related agricultural damage claims between 2015 and 2022. *Source:* Lechner Knowledge Center, based on the Agricultural Risk Management System (MKR).

In connection with the 2022 drought, a new regional study over the operational area of the Trans-Tisza Region Water Directorate (TIVIZIG) located in the northern part of the Great Plain was performed by Zs. Hetesi and T. Bódi. They examined the change in the contiguous duration of rain-free days

between 1964–1989 and 1990–2022 during the vegetation period, using the data of the 15 measuring stations of TIVIZIG. The alternative hypothesis of the research was that the distribution of extremely long (>25 days) rain-free periods differs between the two intervals.

The results of the F-test performed on the data sets with a confidence level of 95% are published here first, showing that a significant difference (increase) occurred in the length of rain-free days between the periods 1964–1989 and 1990–2022 (*Fig. 5*) in the northern part of the Great Plain, which must be taken into account when developing future drought prevention strategies.

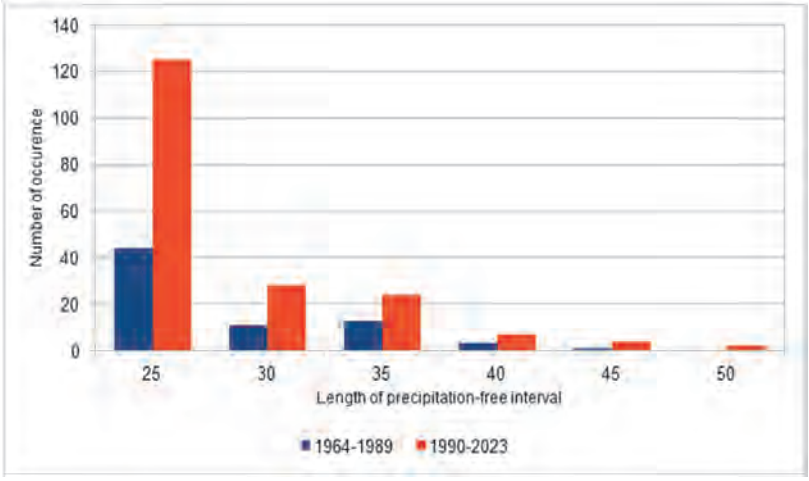

Fig. 5. Length of precipitation-free intervals (expressed in days) for the periods 1964–1989 and 1990–2023. *Source:* based on TIVIZIG measurements

Increasing the proportion of irrigated agricultural land and irrigation development are often mentioned as a way of "solving" the issue of water scarcity and drought damage in agriculture. *Fig. 6* illustrates the trends in agricultural water use between 2000 and 2020, showing that decreasing rainfall is associated with increasing irrigation water use.

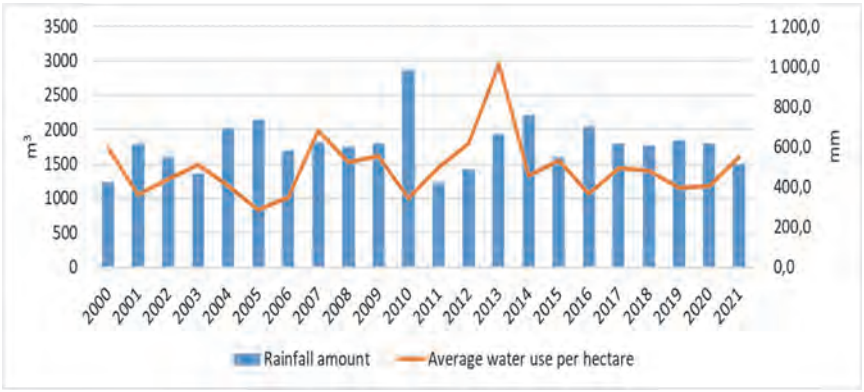

Fig. 6. Trends in agricultural water use between 2000 and 2021. *Source:* KSH data (KSH, 2022c).

However, it is important to stress that irrigation alone cannot solve the problem. As shown in *Fig. 7*, the proportion of irrigated land is orders of magnitude below the drought-affected area. Meeting the needs of the huge water demand of an intensive irrigation development – both in terms of area and water quantity – is not a realistic goal, especially if other conditions are kept unchanged.

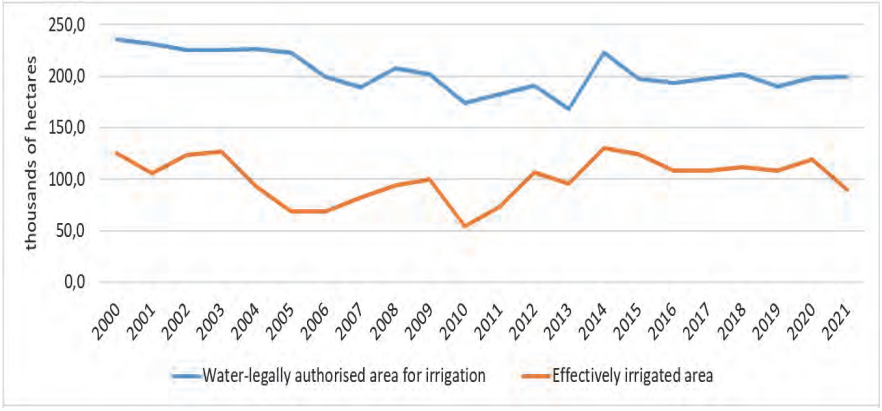

Fig. 7.: The extent of irrigated area between 2000 and 2021. *Source:* KSH data (KSH, 2022c).

Water abstraction for irrigation – calculated on the water deficit of about 1.8–2.2 billion cubic meters of the total irrigable area – can have a significant negative impact on the water flow of rivers at low water periods. In the long term, about 1.5 billion cubic meters of water scarcity and resulting water demand can be expected on the Great Plain (*Jung*, 2022). This amount cannot be replaced from rivers in low water periods; hence, solutions stocking water from the rivers at high water periods are necessary, such as water retention in the landscape and by using artificial structures.

Irrigation or its development is indeed necessary in the case of certain crops (e.g., vegetables), this is the only way to satisfy conditions for their (further) cultivation. However, in the case of field crops, other solutions must also be implemented for the successful adaptation to changing circumstances.

5. Current decision support and planning tools

Geographic Information Systems (GIS) have become a widely used tool for complex analysis and planning tasks involving a wide range of data and spatial relationships. In Hungary, IT systems in various sectors connected to water management (water, nature conservation, agriculture, disaster management etc.) use GIS solutions for everyday tasks. Besides this, GIS is a very efficient tool to solve specific, multi-sectoral problems, permitting easy integration of cross-sectorial data and the expertise.

Data from remote sensing images has become a key in recent decades in several application areas, while rapid development in aerial remote sensing techniques has also enabled high-resolution and high-precision analyses. Aerial photographs and the derived orthophotos, as well as surface and terrain models produced by laser scanning (LIDAR) and other technologies are the cornerstones of any water management planning (*Szabó et al.*, 2017; *Uuemaa et al.*, 2018; *Demelezi et al.*, 2019; *Nagy et al.*, 2020; *Csatáriné et al.*, 2020).

Furthermore, the increasing amount of data yielded by different earth observation satellite systems (e.g., NASA/USGS Landsat missions, https://www.nasa.gov/mission_pages/landsat/main/index.html; ESA/EU Sentinel missions, https://sentinels.copernicus.eu/web/sentinel/home), open data policy, and the decades of available archives of imagery provide a unique opportunity to understand the past and present of a given area. Among others, the nature and condition of vegetation, changes in land cover, extent of surface water, and soil moisture content can all be observed and measured by satellite data, studying a single time or time series of images (*Csornai et al*., 2007; *Mucsi* and *Henits*, 2011; *van Leeuwen et al.*, 2020; *Kozma et al.*, 2022).

In the light of the above, it can be stated that data-driven planning of water retention can most effectively be achieved through systems integrating GIS and

remote sensing tools. The following provides an insight into the solutions currently available for this purpose.

5.1. The Agricultural Risk Management System (MKR)

The fundamental objective of MKR is to provide a unified system for mitigating the economic impact of adverse weather events on agricultural production and to manage compensation for damages (*Act CLXVIII of 2011*, https://net.jogtar.hu/jogszabaly?docid=a1100168.tv). The system handles a complex and multifaceted database, facilitating the work of all actors and processes involved in the compensation process, namely farmers' damage reporting, claims and payments of compensations, insurance, and official controls. MKR also plays a major role in decision-making at management and executive levels (*Nádor et al*., 2018; *NAK*, 2020).

In 2012, the former Institute of Geodesy, Cartography and Remote Sensing (FÖMI) joined the national project for MKR development; the Lechner Knowledge Center (LTK) took over its tasks in 2019. LTK contributes to the effective operation and development of the system by achieving and processing high- and medium-resolution optical satellite images to map and monitor the extent and temporal/spatial frequency of certain phenomena caused by extreme weather events in agricultural areas. LTK produces the following maps and databases:

- operational inland excess water maps for specific dates and periods,
- inland excess water frequency maps,
- drought maps maps indicating anomalies in the values of vegetation indices to characterize crop conditions, and
- drought frequency maps (see more details in Section 5.2).

These data are regularly uploaded to the central database of MKR and shared with other relevant institutions.

5.2. Mapping drought, crop condition, and inland excess water

Mapping of agricultural crop conditions, resulting from more than a decade of research and development in Hungary, plays a fundamental role in drought damage assessment, (*Csornai et al.,* 2006, 2007). Thanks to the continuous research and development activities, crop conditions or drought maps have been improved and adapted to the technologies and data sets currently available and produced in a routine manner for operational use.

Originally, the mapping was based on the processing of medium-resolution MODIS satellite images, as at the launch of the MKR in 2012, the 250 m resolution images of the MODIS sensors (https://modis.gsfc.nasa.gov/about/) on NASA's Aqua and Terra satellites provided the fastest available and openly available data for this task. The maps

consider a time series of optical images from more than 20 years within a given period of the year, typically August, depending on the weather. The spatial resolution of the maps is 250 meters, i.e., one pixel covers an area of approximately 6.25 hectares. Therefore, the maps are not suitable for field-level analyses at typical Hungarian parcel sizes but can be used to identify regional variations.

Besides assessing and estimating the damage in a given year, the long time series (20 years) of satellite data provides an opportunity to produce a drought frequency map (*Fig. 8*) as well, an indicator of high importance for a long-term adaptation to the phenomenon. The map shows a percentage of drought-affected years for each pixel over a 20-year period.

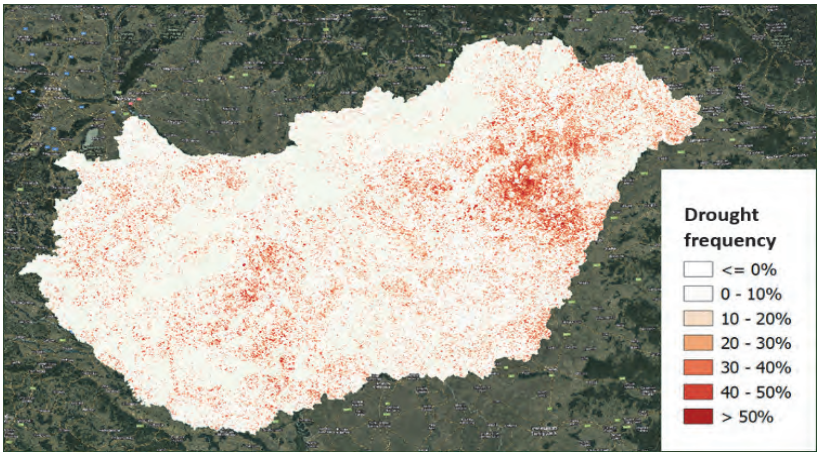

Fig. 8.: National drought frequency map for the second half of August (based on a time series of MODIS satellite images between 2003 and 2022). *Source:* LTK.

In 2021, *Birinyi et al.* (2021) conducted a drought sensibility study on maize fields based on time-series of medium-resolution MODIS images, and from 2022 onwards, methodological developments of crop condition mapping based on high-resolution Sentinel-2A and 2B satellite images have also been started (*Birinyi et al.*, 2022a, 2022b, 2022c). Multiple different spectral indices are calculated from the values measured at different wavelengths, providing information on photosynthetic activity, leaf water content, or the amount of green biomass, thus enabling a complex assessment of local vegetation conditions.

LTK experts also use openly available high-resolution Sentinel-2 and Landsat 8/9 satellite images for operational inland excess water mapping. The spatial resolution of these images allows observations at a sufficient level of detail. The workflow requires high-level expert control for the fine-tuning of mapping thresholds to provide status maps for a given day over the affected areas. Clouds can constitute a major hindrance in the availability of optical images. Depending on the availability of cloud-free imagery, period-integrated inundation maps are also created based on several images taken at different times. The longer-term study of the damage event's impact is ensured by processing satellite images acquired on different dates: a first one as early as possible after inundation, and another several weeks later. The combination of the two produces a so-called persistent excess water map, which provides an adequate characterization of the waterlogging situation in a given area over longer periods. These maps are only made for agricultural areas eligible for area-based payments (SAPS) at a resolution of 10 or 30 meters, depending on the sensor. The categories of the map provide information on the extent of open water surfaces, vegetation standing in water, and waterlogged soil (i.e., saturated with water).

Similarly to the drought frequency map, regularly updated relative inland excess water frequency maps are also provided by LTK. The methodological developments of LTK's predecessor institution, FÖMI, resulted in flood and inland excess water maps for parts of the country and, in certain years, for the whole country, starting from 1998 (*Nádor et al.*, 2018). The most recent map was made by integrating the yearly maps produced in the period of 1998–2021 showing the number of times a certain area was inundated or waterlogged during the study period (*Fig. 9*).

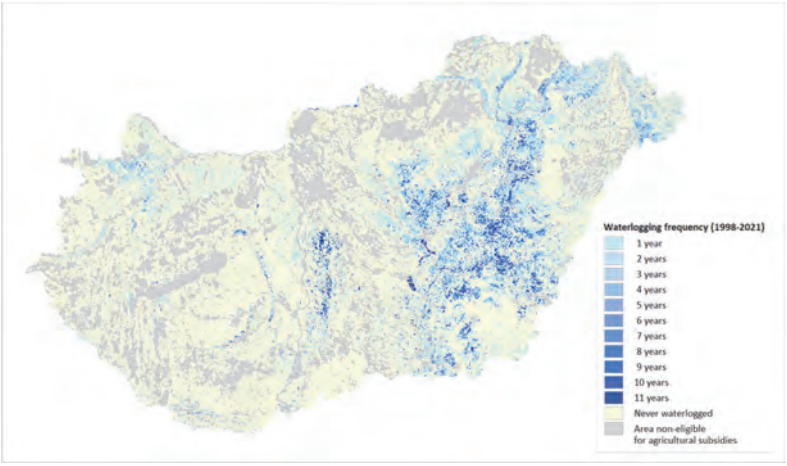

Fig. 9. Country-wide inland excess water / waterlogging frequency map (1998-2021). *Source:* LTK.

5.3. Mapping crop conditions in the extremely dry year of 2022

5.3.1. Drought maps derived from MODIS sensor data

In 2022, responding to the extremely dry weather, LTK started to produce MODIS-based crop condition maps from May on and uploaded them to the MKR central system twice a month until the end of August. To respond quickly, the first maps provided information for all eligible agricultural areas included in LPIS, but later, when claim data became available, the maps were re-generated with bare soil or stubble parcels excluded from the analysis. In total, LTK provided 13 country-wide MODIS-based maps to the MKR from May to August 2022 (*Fig. 10*).

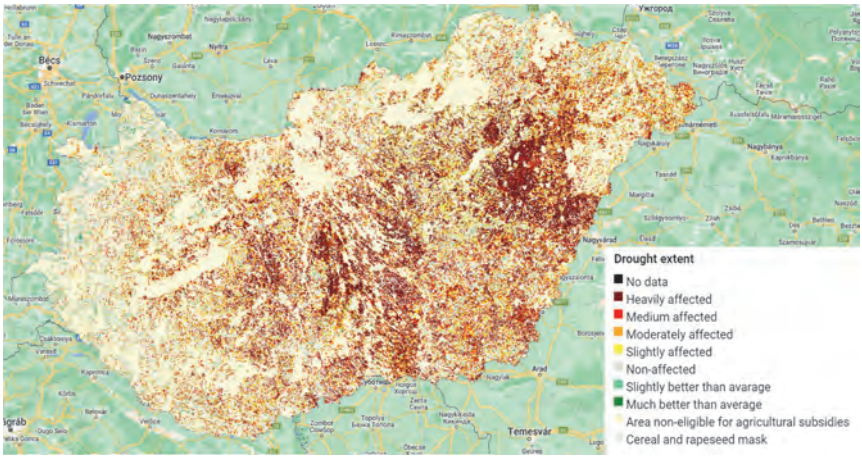

Fig. 10. Drought extent in the first half of August, 2022. *Source:* LTK.

5.3.2. Development of high-resolution crop condition maps

In 2022, LTK experts developed a methodology for integrating high-resolution Sentinel-2 (A and B) satellite imagery in crop condition mapping *(Birinyi et al.*, 2022c). These satellites of the European Union (EU) and European Space Agency (ESA) provide optical images with spatial resolutions of 10, 20, and 60 meters every 2-3 days, which could be used to significantly increase the level of detail of resulting maps. It is a promising direction for the MKR in laying the foundation for parcel-level or even more detailed drought mapping, and the results could also contribute to supporting data collection for the new

Common Agricultural Policy (CAP) (*EU Regulation 2021/2115*, https://eur-lex.europa.eu/legal-content/EN/TXT/?uri=CELEX%3A32021R2115). However, the method requires further validation to prepare the operational use of results.

The most significant outcome of this research is the ability to provide high-resolution crop condition maps, specific in terms of location, time, and crop type. The underlying methodology is based on the integrated analysis of multiple different spectral indices including three vegetation indices, a moisture content index, and a yellowness index. The map identifies six condition categories depending on the number of indices showing values worse than those typical for the given crop in similar periods in previous years in the given area. The results were shared with the National Food Chain Safety Office (NÉBIH) for four different periods and two agricultural crops (maize and sunflower) during the summer of 2022 to assess operational application. Besides this, ground truth was also collected by LTK experts in five locations in August 2022 over 250 sample points for quantitative validation and fine-tuning. Although detailed investigations are still ongoing, field visits and expert feedback so far indicate that the categories correspond well to plant conditions observed on the field (*Fig. 11).*

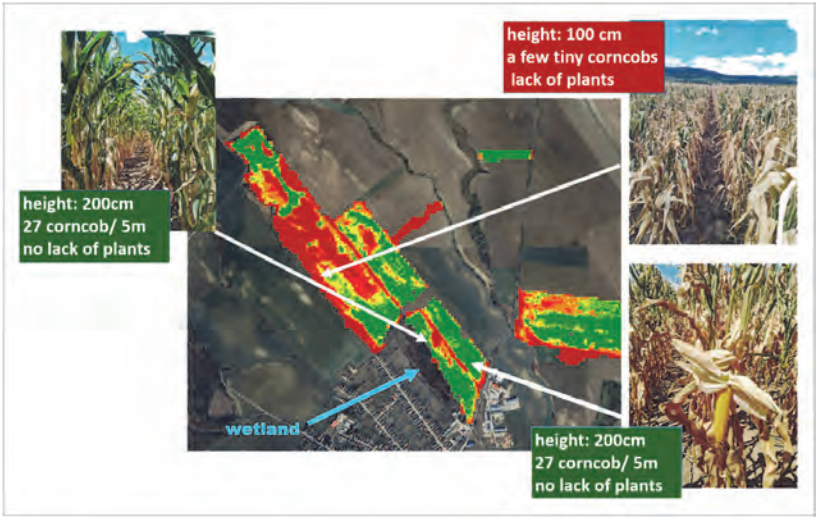

Fig. 11. Pattern of the high-resolution crop condition map and its correlation to on-the-spot observations. *Source:* LTK.

Fig. 12a and *12b* introduce some map extracts on the example of maize.

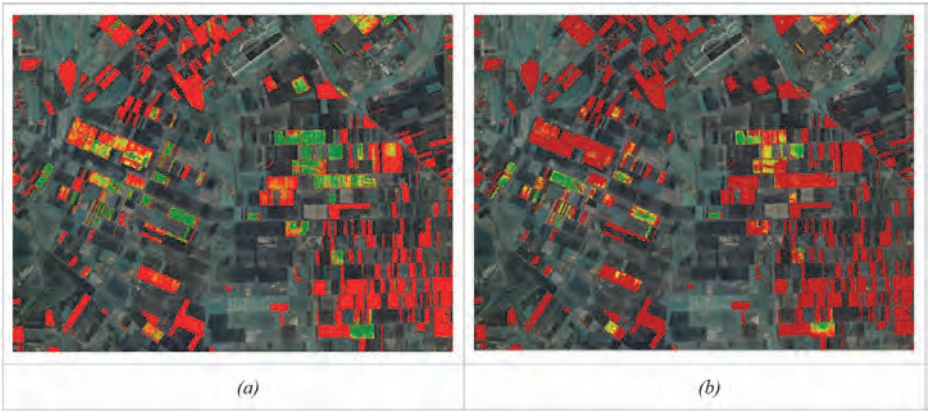

Fig. 12. Illustration of the high-resolution crop condition map: maize fields in the surrounding area of Karcag, on July 3, 2022 (a) and July 23, 2023 (b). Crops in worse condition than in previous years appear in yellow, those in much worse condition in red. *Source:* LTK.

5.3.3. Soil moisture data from space

In addition to damage assessment and monitoring, satellite sensors can potentially be used for forecasting, considering that soil moisture (among other factors) at any given time has a significant influence on subsequent plant conditions.

Passive microwave sensors (e.g., SMOS mission https://earth.esa.int/eogateway/missions/smos; SMAP mission https://smap.jpl.nasa.gov/mission/description/) can be used to monitor soil moisture status from space (*Eswar et al.*, 2018*; Remote Sensing Special Issue*, 2023). Although the spatial resolution of these data is small, at the same time they provide frequent revisits. For example, the processing chain of NASA's SMAP (Soil Moisture Active Passive) satellite, operating since 2015, provides modeled soil surface and subsurface moisture values with a spatial resolution of 9 kilometers almost every day. Besides the “usual” summer drought period, these data also contribute to monitoring the increasingly frequent "spring drought" events to a great extent (*Fig. 13*). The latter are the consequence of the decrease in winter precipitation and the lack of slowly melting snow cover. *Fig. 13* illustrates the phenomenon on SMAP soil moisture values for February 2022, when the soil was significantly drier compared to the same period of the previous year, especially in the country's eastern regions.

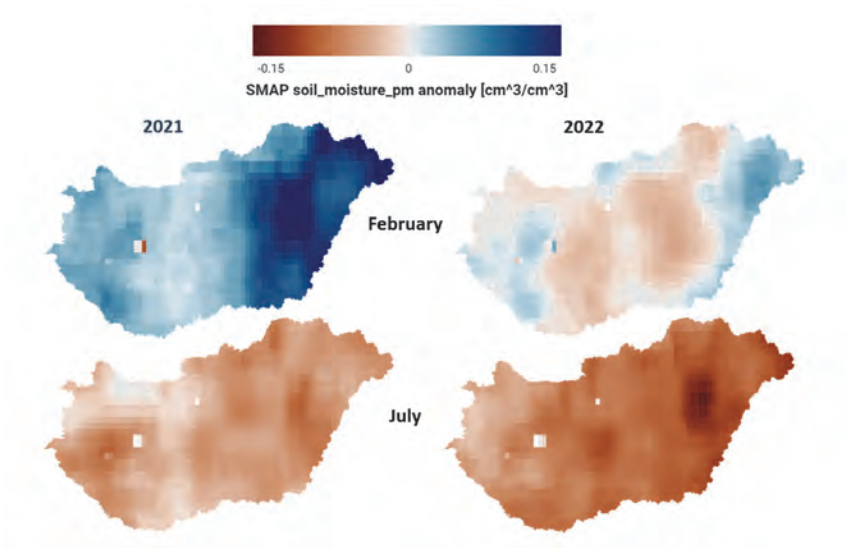

Fig. 13. Soil moisture anomalies based on SMAP data in late winter and summer in 2021 and 2022. *Source:* NASA, SMAP / Google Earth Engine / LTK.

When comparing SMAP soil moisture of the years 2021 and 2022, the difference in moisture deficit is striking between the western counties (e.g., Zala), covered with forest mosaic, and the eastern half of the country, predominantly composed of arable lands (e.g., Jász-Nagykun-Szolnok county), especially in early spring 2022. Although this difference had largely disappeared by August 2022, the conditions under which agricultural crops could develop during the main growing period were spectacularly different (*Fig. 14*).

When used carefully and thoroughly, the above methods and instruments can support the reconsideration of the current practice and the development of a more sustainable, integrated, and water-efficient land management with consideration of all ecosystem cascade services that human life is based on.

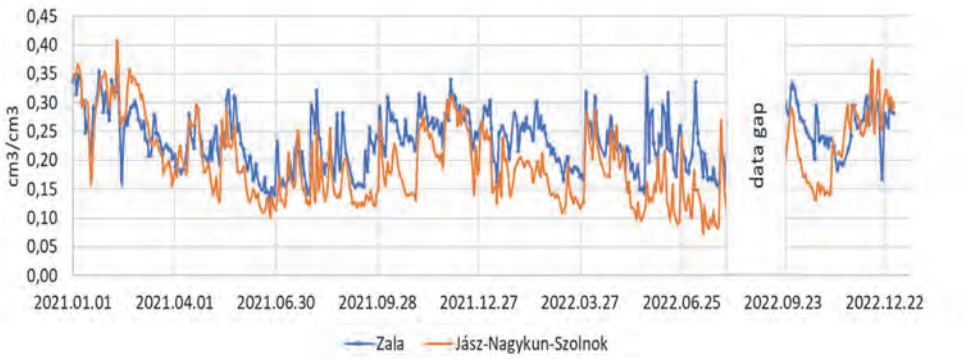

Fig. 14. Time series of SMAP surface soil moisture data for years 2021 and 2022 for two Hungarian counties (Zala and Jász-Nagykun-Szolnok) showing significantly different moisture conditions. *Source:* LTK, based on SMAP data.

6. Summary, recommendations

According to the "Global Risk Report 2023" released by the Davos World Economic Forum, "Climate action failure" stands on the first and the second places of global risks overall (*WEF*, 2023).

In order to adapt to the extreme weather effects expected in the Carpathian Basin, it is crucial to introduce sustainable land and water management by restoring the relationship and ensuring proper balance and efficient fluxes among precipitation, soil conditions, vegetation, crops and water, nutrients, and evaporation (*O.Lakatos et al.*, 2022).

6.1. Soil health

6.1.1. No till

In order to heal the framework of soil conditions–vegetation–crop and water–nutrients–evaporation, the first necessary step is the wide-scale introduction of soil-conserving cultivation techniques, including the abandonment of plowing as much as possible.

The essence of the method is that with the mindful use of cover crops and the absence of plowing, a deeper, structured layer is formed in the soil, permitting the retention of a larger amount of precipitation and a deeper penetration of rainwater into the soil, making it capable of retaining up to 100% more rainwater (*Hetesi*, 2019).

6.2. Land cover change, mulching in agriculture

6.2.1. Buffer strips, installation of agro-forestry systems

Buffer strips are areas of natural vegetation cover (grass, bushes, or trees) at the margin of fields, arable land, transport infrastructures, and water courses. They can have several different configurations of vegetation types, varying from grass-only to different combinations of grass, trees, and shrubs. Due to their permanent vegetation, buffer strips offer good conditions for effective water infiltration and slowing down surface flow; they, therefore, promote the natural retention of water. They can also significantly reduce the amount of suspended solids, nitrates and phosphates originating from agricultural run-off. Buffer strips can be located in riparian zones, or further away from water bodies as field margins, headlands, or even within fields (e.g., beetle banks). Hedges across long, steep slopes may reduce soil erosion as they intercept and slow down surface run-off water before it builds into a damaging flow, particularly where there is a margin or buffer strip alongside (NWRM website, http://nwrm.eu/measure/buffer-strips-and-hedges).

6.3. Water management by creating place for it with a mosaic landscape structure

Where the potential evaporation is greater than the available precipitation, there is no harmful water, only water that has no place. The problems of inland excess water and drought are largely caused by the fact that the current water management approach is territorially minimized, as there is literally no place for water.

Water replacement must be built on spreading floods and retaining inland excess waters. It requires a mosaic landscape structure and a management practice that matches landscape features. Mosaicism means that water replacement and the formation of local waterlogging can be solved by re-creating temporary or permanent wetlands in areas that are essentially not suitable for agricultural cultivation. A dominant proportion of these areas was originally waterflow or largely water-affected land.

Landscape use oriented at water buffering (i.e., acquiring excess water and returning it in a natural way) could also save the conditions for arable farming. As an estimate, 2/3 of the current production can be secured by the extensive transformation of arable land.

A reasonable territorial compromise can be a solution to the problems that have arisen, during which nearly half a million hectares of land along the Tisza – least suitable for intensive production – would be returned to the landscape, for sustainable landscape management. The Tisza valley, therefore, does not need artificial reservoirs but hundreds of thousands of hectares of flood plain (*Balogh*, 2022; *Murányi* and *Koncsos*, 2022).

A few thoughts on irrigation: replenishment of water-deficient areas can be solved primarily from the low water flow rivers. Due to the characteristics of our country, we currently do not have areas suitable for water reservoirs where we could retain and store large amounts of irrigation water. Reservoirs in the river bed, e.g., above Tiszalök, and the existing reservoirs, such as Lake Tisza, are not primarily used to hold back large amounts of water, but rather to provide a short-term buffer and to enable gravity water withdrawals. If the water from these reservoirs were to be used for irrigation during a prolonged period of water shortage, gravity water extraction above Tiszalök would be impossible.

Withdrawal of irrigation water can significantly affect the small water yield of rivers in an unfavorable direction, with the totality of irrigable areas requiring approximately 1.8–2.2 billions of cubic meters based on their calculated water deficit. Looking at the long-term processes, we can expect a water deficit of around 1.5 billion m^3 in the Great Plain of Hungary, and consequent water demand. This quantity cannot be replenished from the water of the rivers during low water periods. Artificial and landscape water retention is therefore necessary, which mainly taps the high water flows.

6.4. Data-based planning

Besides global and local weather conditions and their variability, several interacting factors influence water balance in the landscape and its hydrological extremes (e.g., drought, inland excess water), such as:

- surface and groundwater conditions and their changes,
- topography, morphology (runoff, water retention),
- soil conditions (water storage capacity, drought sensitivity, etc.),
- type of land cover (evaporation, cooling capabilities, erosion prevention, etc.),
- type of land use and cultivation (soil conservation, soil structure retention, preventing soil degradation, erosion control, etc.),
- hydrology of the area, water balance, water quality,
- the 'history' of the landscape, both in terms of hydrology and land-use change (the key to solving water retention issues is often rooted in this),
- other current landscape characteristics (e.g., built-up areas, land reclamation, the impact of water works and water management, etc.),
- ownership tenure,
- regulatory regime, legislative framework,
- data policy,
- et cetera.

Therefore, mapping damage events related to climate change and their consequences, modeling and identifying areas at risk and development of adequate solutions require the close cooperation of several disciplines and areas of expertise, including governmental and non-governmental organizations and people working to solve local problems, including farmers.

To develop strategies on both local and national levels, it is essential to acquire a thorough understanding of all these factors, and to carry out conscious planning based on all relevant data and knowledge.

So far, data collected in various sectors by research institutes, measurement networks, or field surveys have resulted in the establishment of large specific information systems, e.g., in the fields of water, meteorology, soil, nature conservation, forestry, land registry, land parcels, etc. In certain areas, though, there is a need for further surveys and mapping activities; for example, a unified national inventory of grasslands and wetlands would serve climate policy as well as agricultural and nature conservation efforts to a great extent.

Besides this, several professional and research institutes build in their practice the multi-purpose use of airborne data (LIDAR, hyperspectral or orthoimages) and medium- and high-resolution satellite images, mainly those freely available from the European Space Agency (ESA) and NASA to solve national and regional or local tasks.

Together with the databases and processing methods mentioned above, the long-time series of remote sensing images can provide a solid basis for trend analysis, anomaly detection, and modeling. All of these data and techniques should play a significant role in the long-term strategic development of climate change adaptation, responding to and monitoring of ad hoc phenomena (e.g., force majeure), and for revealing cause and effect relationships.

Numerous research institutes are at the forefront of state-of-the-art data processing, with machine learning and artificial intelligence algorithms being applied by almost all national research and R&D laboratories with expertise in meteorology, soils and water management, land cover and land use monitoring, ecology and vegetation research. With this experience, these laboratories and institutes can effectively contribute to the preparatory studies for a strategy or to solve specific problems of smaller regions.

In connection with the above, we draw attention to all the research on landscape history, as well as to the proposals of organizations, people, and farmers working on local issues; those, by involving invaluable local knowledge, offer reasonable solutions for the questions about where and how to preserve the water in the landscape.

So, the data and expertise are given, but harmonized use of them faces many difficulties.

Droughts and floods, among many other phenomena, are the "output products" of a complex, systemic problem, which is global climate change, combined with often inappropriate land use practices. Responding to these

phenomena requires complex thinking, greater interoperability of information systems, and closer cooperation between disciplines, local farmers and land users. An integrated decision support system can hardly develop in the right direction (or fast enough) with an insufficient stream of information or without mutual feedback among underlying information systems and disciplines. For instance, assessment of crop conditions and payment of compensations should be integrated with the analysis of satellite imagery along with soil and meteorological conditions and compensation claims. Likewise, delineation and management of areas suitable for water retention should be based on landscape characteristics and integrated with water management and land consolidation.

Currently, in Hungary, the low degree of interoperability – mainly due to the rigid data policy – constitutes a major hindrance for rapid response and effective solutions for situations resulting from the climate crisis.

References

Arcanum Adatbázis Kiadó, 2023: Történelmi térképészeti felmérések digitális adatbázisa (Database of historical cartographic surveys) [online] https://maps.arcanum.com/hu/browse/country/. Accessed on 15/06/2023.

Babinszki, E., 2017: Térképek a múltból: Pocsolyatérkép. *Élet és tudomány 29*, 15–17. (In Hungarian)

Balogh, P., 2001: Az ártéri tájgazdálkodás koncepciója (Előleges javaslat). *Földrajzi Közlemények 2001*, 249-270. (In Hungarian)

Balogh P., 2022: Vízválasztó konferencia tézisgyűjtemény és szakmai szakmai jelentés. Vízválasztó Konferencia, Agrárminisztérium, 202209.23. [online] https://s3-eu-central-1.amazonaws.com/elotiszaert.hu/wp-media-folder-elotiszaert-hu/wp-content/uploads/2022/09/vizvalaszto-konferencia-szakmai-jelentes-h1f3sz.pdf Accessed on 10/06/2023.

Birinyi, E., Kristóf, D., Barcza, Z., and *Kern, A.*, 2021: Vegetációs indexek és meteorológiai tényezők idősorainak aszálydetektálási célú vizsgálata különböző hazai termőtájakon, kukorica haszonnövényre. In (Ed.: *Molnár V.É)* Térinformatikai Konferencia és Szakkiállítás XII. Debrecen. Az elmélet és a gyakorlat találkozása a térinformatikában 2021, 67–68. https://giskonferencia.unideb.hu/arch/GIS_Konf_kotet_2021.pdf

Birinyi, E., Kristóf, D., Kern, A., Rotterné Kulcsár, A., and *Barcza, Z.*, 2022a: A Mezőgazdasági Kockázatkezelési Rendszerbe benyújtott aszály kárigények nagyfelbontású műholdfelvételekkel történő igazolhatóságának vizsgálata - kezdeti lépések, In *(Eds.: Molnár, D.* and *Nagy, A. Sz.)* Tavaszi Szél 2022 *Tanulmánykötet I. Budapest, Magyarország: Doktoranduszok Országos Szövetsége* (DOSZ), 179–196. (In Hungarian)

Birinyi, E., Kern, A., Barcza, Z., and *Kristóf, D.*, 2022b: A mezőgazdasági kockázatkezelési rendszerbe benyújtott aszály kárigények igazolhatóságára rendelkezésre álló sentinel-2 felvételek a jogszabályi határidők betartásával. *Egyetemi Meteorológiai Füzetek: Az éghajlatváltozás és hatásainak vizsgálata, levegőminőségi elemzések: No. 34.* 13–21. (In Hungarian) https://doi.org/10.31852/EMF.34.2022.013.021

Birinyi, E., Kern, A., Kristóf, D., and *Barcza, Z.*, 2022c: Nagyfelbontású kukorica és napraforgó állapot-térképezés a Mezőgazdasági Kockázatkezelési Rendszerben: a 2022-es aszály hatása. In (Ed.: *Molnár V.É.*) Az elmélet és gyakorlat találkozása a térinformatikában XIII. Debreceni Egyetemi Kiadó 75–81. (In Hungarian)

Csatáriné Szabó, Z., Mikita, T., Négyesi, G., Varga, O.G., Burai, P., Takács-Szilágyi, L., and *Szabó, S.*, 2020: Uncertainty and Overfitting in Fluvial Landform Classification Using Laser Scanned Data and Machine Learning: A Comparison of Pixel and Object-Based Approaches. *Remote Sens. 12*, 3652. https://doi.org/10.3390/rs12213652

Csornai, G., Wirnhardt, Cs., Suba, Zs., Nádor, G., Tikász, L., Martinovich L., Kocsis, A., Zelei, Gy., László, I., and *Bognár, E.*, 2006: CROPMON: Hungarian crop production forecast by remote sensing. ISPRS Archives XXXVI-8/W48 Workshop proceedings: Remote sensing support to crop yield forecast and area estimates. 25–30. https://www.researchgate.net/publication/265430682_CROPMON_Hungarian_crop_production_forecast_by_remote_sensing

Csornai, G., Suba, Zs., Nádor, G., László, I., and *Wirnhardt, Cs.*, 2007: Disaster monitoring with the integrated utilization of ENVISAT and other satellite data sets in the 2004-2006 period in Hungary, ESA ENVISAT Symposium, Montreux, 23-27 April, 2007.

Demelezi, F., Galya, B., Tamas, J., Demelezi, I., and *Nagy, A.*, 2019: Evaluation of soil water management properties based on LIDAR data and soil analyses at farm level, *Nat.Resour. Sustain. Develop. 9*(2), 160-173. https://doi.org/10.31924/nrsd.v9i2.033

De Vries, F.T., Hoffland, E., van Eekeren, N., Brussaard, L., and *Bloem, J.*, 2006: Fun- gal/bacterial ratios in grasslands with contrasting nitrogen management. *Soil Biol. Biochem. 38*, 2092–2103. https://doi.org/10.1016/j.soilbio.2006.01.008

Dobos, E., 2022a: Katasztrofális a magyar talajok állapota, és ezért nagy árat fizetünk. *Agroinform, 2022*. március 27. [online] https://www.agroinform.hu/szantofold/dobos-endre-interju-talajszerkezet-humusz-szerves-anyag-55159-001?&hash=344d802c6aa3d97c465ccf82103cd3a5. Accessed on 15/06/2023. (In Hungarian)

Dobos, E., 2022b: A talajok és a talajdegradáció szerepe a szélsőséges vízgazdálkodási helyzetek kialakulásában *Vízügyi Közlemények CIV. 2022 3.* https://talajtar.hu/dobos-endre-a-talajok-es-a-talajdegradacio-szerepe-a-szelsoseges-vizgazdalkodasi-helyzetek-kialakulasaban/ (In Hungarian)

Eswar, R., Das, N.N., Poulsen, C., Behrangi, A., Swigart, J., Svoboda, M., Entekhabi, D., Yueh, S., Doorn, B., and *Entin, J.*, 2018: SMAP Soil Moisture Change as an Indicator of Drought Conditions. *Remote Sensing 2018*, 10, 788. https://doi.org/10.3390/rs10050788

Hetesi, Zs., 2019: Systematic and Simple Cost-Benefit Investigation of Some Advantages of the Regenerative Agriculture. *Region. Business Stud. 11*, 7–11. https://doi.org/10.33568/rbs.2401

Horváth, R., 2018: Árpád-kori ökológia. Árokrendszer és vízgazdálkodás. In: (Ed.:*Kocsi L.*) Ars Naturae. Tanulmányok, esszék, előadások ember és környezetének kapcsolatáról. 5. Vol.8–9(15–18) 19–26. (In Hungarian) https://www.agroinform.hu/szantofold/dobos-endre-interju-talajszerkezet-humusz-szerves-anyag-55159-001?&hash=344d802c6aa3d97c465ccf82103cd3a5

NAK, 2020: *Hungarian Chamber of Agriculture:* Bővül a mezőgazdasági kárenyhítési rendszer (Expansion of the Agricultural Risk Management System). [online] www.nak.hu/en/tajekoztatasi-szolgaltatas/mezogazdasagi-termeles/102092-bovul-a-mezogazdasagi-karenyhitesi-rendszer Accessed on 01/07/2023 (In Hungarian)

Jung I. 2022: Öntözött területek Magyarországon - helyzetelemzés. *Magyar Mezőgazdaság, 2022. augusztus 18.* [online] https://magyarmezogazdasag.hu/2022/08/18/ontozott-teruletek-magyarorszagon-helyzetelemzes Accessed on 25/06/2023. (In Hungarian)

Kiedrzyńska, E., Kiedrzyński, M. and *Zalewski, M.*, 2015: Sustainable floodplain management for flood prevention and water quality improvement. *Nat. Hazards 76*, 955–977. https://doi.org/10.1007/s11069-014-1529-1

Kis, A., Pongrácz, R., and *Bartholy, J.*, 2017: Multi-model analysis of regional dry and wet conditions for the Carpathian Region. *Int. J. Climatol. 37*, 4543–4560. https://doi.org/10.1002/joc.5104

Kozma, Z., Jolánkai, Zs., Kardos, M.K., Muzelák, B., and *Koncsos, L.*, 2022: Adaptive Water Management-land Use Practice for Improving Ecosystem Services – a Hungarian Modelling Case Study. *Periodica Polytechnica Civil Engineering, 66(1)*, 256–268. https://doi.org/10.3311/PPci.18369

KSH, 2022a: Area exposed to drought. [online] https://www.ksh.hu/stadat_files/kor/en/kor0039.html Accessed on 15/06/2023.

KSH, 2022b: Sustainable Development Goals: Flood and inland inundation. [online] https://www.ksh.hu/sdg/3-20-sdg-15.html Accessed on 15/06/2023.

KSH, 2022c: Water use in agriculture. [online] https://www.ksh.hu/stadat_files/mez/en/mez0046.html Accessed on 01/06/2023

Makarieva, A.M., Gorshkov, V. G. and *Li, B-Li.*, 2005: Biochemical universality of living matter and its metabolic implications. *Functional Ecol. 19*(4), 547–557. https://doi.org/10.1111/j.1365-2435.2005.01005.x

MBFSZ, 2023: Water-covered and flood-prone areas of the Carpathian Basin before the start of the relief and drainage works [online] https://map.mbfsz.gov.hu/terkepekamultbol/Mo_arviz_1938/ Accessed on 15/06/2023.

MKR, 2022: Hungarian Ministry of Agriculture Agricultural Risk Management System (MKR) databases 2015–2022

Molnár, G., 2005: Az ártéri gazdálkodás elmélete és a gyakorlati megvalósítás terve egy konkrét mintaterületen. Bokartisz kiadó. https://s3.eu-central-1.amazonaws.com/elotiszaert.hu/wp-media-folder-elotiszaert-hu/wp-content/uploads/2020/01/arteri_taj05_nezo.pdf (In Hungarian)

Mucsi, L., and *Henits, L.*, 2011: Belvízelöntési térképek készítése közepes felbontású űrfelvételek szubpixel alapú osztályozásával. *Földrajzi Közlemények 135*(4), 365–378. https://foldrajzitarsasag.hu/downloads/foldrajzi_kozlemenyek_2011_135_evf_4_pp_365.pdf (In Hungarian)

Murányi G. and *Koncsos L.*, 2022: Tározási alkalmasságok az Alföldön. Vízátvezetés, vízvisszatartás, vízpótlás. Magyar Hidrológiai Társaság vándorgyűlése, Nyíregyháza, Hungary 2022. July. (In Hungarian)

Nagy, G., Lóczy, D., Czigány, Sz., Pirkhoffer, E., Fábián Sz.Á., Ciglič R., and *Ferk, M.*, 2020: Soil moisture retention on slopes under different agricultural land uses in hilly regions of Southern Transdanubia. *Hungarian Geograph. Bull. 69*(3) 263–280. https://doi.org/10.15201/hungeobull.69.3.3

Nádor, G., Friedl, G., Rotterné Kulcsár, A., Hubik, I., Pacskó, V., and *Surek, Gy.*, 2018: Agricultural damage mapping in Hungary (in) The ever-growing use of COPERNICUS across Europe's regions. *EC, ESA and NEREUS.* 44–45. https://www.nereus-regions.eu/wp-content/uploads/2017/10/PUBLICATION_Copernicus4regions_2018.pdf

O.Lakatos B. and *Ungvári G.*, 2022: Ökoszisztéma szolgáltatások koncepciója a vízgazdálkodásban *Hidrológiai Közlöny 102*(3) 4–19. http://www.hidrologia.hu/mht/letoltes/HK2022_03.pdf#page=6 (In Hungarian)

OVF, 2019: Jelentős vízgazdálkodási kérdések. Magyarország vízgyűjtő-gazdálkodási tervének második felülvizsgálata. 29 p. [online] Accessed on 01/07/2023. (In Hungarian) https://vizeink.hu/wp-content/uploads/2020/12/JVK_2019_Vegleges.pdf

OVF, 2021: A harmadik Országos Vízgyűjtő-gazdálkodási Terv Stratégiai Környezeti Vizsgálata 161 p. [online] Accessed on 01/07/2023 (In Hungarian) https://vizeink.hu/wp-content/uploads/2022/10/skv/VGT3_SKV_vegleges.pdf

OVF, 2022: Magyarország vízgyűjtő-gazdálkodási terve - 2021. 712 p. [online] Accessed on 01/07/2023 (In Hungarian) https://vizeink.hu/vizgyujto-gazdalkodasi-terv-2019-2021/vgt3-elfogadott/

Pálfai I., 2000: A víz szerepe és jelentősége az Alföldön, A Nagyalföld Alapítvány kötetei *6.* Békéscsaba. (In Hungarian) chrome-extension://efaidnbmnnnibpcajpcglclefindmkaj/ http://acta.bibl.u-szeged.hu/63886/1/nagyalfoldi_006.pdf

Remote Sensing Special Issue 2023: "Remote Sensing of Soil Moisture for Agricultural Purposes" 31 July 2023 https://www.mdpi.com/journal/remotesensing/special_issues/soil_moisture_agricultural_purpose

Szabó, Z., Tóth, C.A., Tomor, T., and *Szabó, S.* 2017: Airborne LiDAR point cloud in mapping of fluvial forms: a case study of a Hungarian floodplain. *GIScci. Remote Sens. 54*, 862–880. https://doi.org/10.1080/15481603.2017.1339987

Torma, Cs.Zs., Kis, A., and *Pongrácz, R.*, 2020: Evaluation of EURO-CORDEX and Med-CORDEX precipitation simulations for the Carpathian Region: Bias corrected data and projected changes. *Időjárás, 124*, 25–46. https://doi.org/10.28974/idojaras.2020.1.2

Uuemaa, E., Hughes, A.O., and *Tanner, C.C.*, 2018: Identifying Feasible Locations for Wetland Creation or Restoration in Catchments by Suitability Modelling Using Light Detection and Ranging (LiDAR) Digital Elevation Model (DEM). *Water 10*, 464. https://doi.org/10.3390/su12072854

van Leeuwen, B., Tobak, Z. and *Kovács, F.*, 2020: Sentinel-1 and -2 Based near Real Time Inland Excess Water Mapping for Optimized Water Management. *Sustainability 2020, 12(7),* 2854. https://doi.org/10.3390/su12072854

VIZITERV Environ Kft.: Comprehensive analysis to determine water management measures to improve drought risk and climate adaptation capacity for the VGT-3/IVOT draft - foundational background material.

WEF, 2023: *World Economic Forum:* The Global Risks Report, 18th Edition. Switzerland. https://www3.weforum.org/docs/WEF_Global_Risks_Report_2023.pdf

DOI:10.28974/idojaras.2023.4.2

IDŐJÁRÁS

Quarterly Journal of the Hungarian Meteorological Service
Vol. 127, No. 4, October – December, 2023, pp. 447–457

Evaluating dehazing techniques on artificial and satellite land surface images

András Fridvalszky*, **Balázs Tóth**, and **László Szécsi**

Department of Control Engineering and Information Technology,
Faculty of Electrical Engineering and Informatics
Budapest University of Technology and Economics
Műegyetem rkp. 3, H-1111, Budapest, Hungary

**Corresponding author E-mail: fridvalszky@iit.bme.hu*

(Manuscript received in final form September 12, 2023)

Abstract— Many image-based recognition tasks are highly susceptible to different types of natural phenomena like foggy weather, snow, or rain. The participating media will likely obscure important details necessary for these algorithms to work correctly. Still, these aspects could be recovered in certain situations with prior information about the underlying light interactions. This could be done with certain heuristics or with the nowadays popular deep-learning based methods. In this paper, we review and compare the results of two approaches to remove or scale down the effects of foggy weather. We also examine how these results can be applied to high resolution satellite images of land surfaces.

Key-words: dehazing, fog, clouds, satellite images

1. Introduction

Fog removal or dehazing is a popular problem nowadays. One example of usage is autonomous vehicles and the corresponding computer vision task, as the artificial intelligence must operate the vehicle with high safety even in the worst visibility conditions. Instead of trusting the machine learning algorithms to solve these problems using diverse data sets, we can help these algorithms by formulating a separate problem. That is to produce a clear output image without the visibility impairing effect from a single input image. It is also important that we must do this with high performance on multiple images, as this is just basically a preprocessing step. The same idea also applies to satellite images. These images are often used to survey, observe, and analyze agricultural areas or vegetation changes, but foggy weather or clouds can be detrimental to their usefulness.

In this paper, we are not introducing another novel algorithm to solve this problem, as there are existing approaches with multiple different ideas. Instead, we turn our attention to the evaluation and analysis of a deep-learning based solution, comparing it to a more traditional idea. We also describe the synthetic training data generation used to train the neural network and how it affects the results.

2. Fog removal techniques

Now we shall discuss the previously mentioned approaches. The first method is based on the work of *He et al.* (2010) and uses a dark channel prior to estimate the contribution of haze that is present on the image. The other technique uses a convolutional neural network to compute an image without fog from the original input picture. It was designed and proposed by *Li et al.* (2017).

2.1. Approach with dark channel prior

Haze (or fog) reduces the light radiance L reflected off surfaces according to the haze transparency (also called transmission). It also adds its contribution to the image, called airlight (denoted by A). The result of radiance reduction and added color is that the original object's radiance is faded, and image value I is different from surface radiance L. Dehazing aims to reconstruct the original surface color L from I as if haze was not there. Dehazing is an ill posed problem, because there is no information in the image about the haze and airlight and where they can be seen. Thus, certain assumptions must be made in order to recover this missing information from the image. In the implemented method, the most fundamental assumption is the “dark channel existence”, which means that the neighborhood of every pixel contains a pixel that should have zero radiance without haze on the examined wavelength. This assumption is reasonable because of the high

frequency of highly saturated color objects, and also because of the existence of shadows. The approach is defined as follows:

$$D = min_B(I) \, , \tag{1}$$

where *D* is the dark channel value, *I* is the image value, *B* is the color channel of RGB image.

Unlike in the original paper proposing the dark channel prior, we evaluate the dark channel and the airlight separately on the red/green/blue wavelengths. This approach is less robust than the original but allows us to handle colored haze, fog, and homogeneous smoke.

The dark channel, according to our assumption, should be zero in haze-free, real-life images. In the case of haze, the dark channel is modified by the airlight, which allows us to estimate the airlight and the haze contributing to the image. More formally, we assume that the minimum radiance must be the haze contribution in any neighborhood.

Knowing the airlight, the transmission can be estimated, which is further refined by the color variation of the original image with the guided filter. Finally, we can subtract the haze and amplify the remaining colors. In the following subsections, these steps are analyzed in detail.

2.1.1. Dark channel computation

The minimum radiance in the neighborhood of each pixel is called the dark channel. The neighborhood is defined by a box filter. For efficiency reasons, we exploit the separability of minimum and average filters, i.e., the 1D versions are executed two times, once for horizontal, and once for vertical direction. This way, the complexity can be reduced from N^2 to *2N*, where *N* is the edge size of the box.

2.1.2. Airlight estimation

The second step is to find out the airlight, i.e., the atmospheric illumination. If no object were visible in a given direction, then we would see this airlight. So pixels are candidates for showing the airlight if their dark channel value *D* is high, i.e., the neighborhood is not dark, and its intensity *I* is also high. Based on these two parameters, we obtain a single comprehensive parameter *F* that describes both components as

$$F = \frac{2DI}{D+I} \, , \tag{2}$$

and select the average intensity *I* of pixels that have the highest *F* parameter:

$$A = \text{avg}_{F \text{ in top } 0.1\%}(I) \, . \tag{3}$$

Our implementation builds up the histogram of the comprehensive parameter *F* on the GPU (graphic processing unit) and selects the top elements on the CPU (central processing unit). As histogram building requires atomic additions, it is done in two steps. First, GPU multiprocessors create partial histograms in their shared memories, and then these partial histograms are merged into a global histogram stored in the main memory. Having read the histogram back to the CPU memory, we read its bins starting from the highest intensity until 0.1% of the number of pixels are included. The airlight is the average of the intensities belonging to this top 0.1% category.

2.1.3. Approximate transmission estimation

Having the airlight *A*, we can determine the transparency, i.e., transmission *t* of the haze at each pixel. Note that, in the dark channel, we only have the contribution of the airlight, and the own contribution of the surface is assumed to be zero, i.e.,

$$D = (1 - t)A\,. \tag{4}$$

From this, the transmission *t* associated with this pixel is

$$\mathrm{t} = 1 - \frac{\mathrm{D}}{\mathrm{A}}\,. \tag{5}$$

Removing all haze typically results in unnatural images, so we introduce a removed haze parameter ω of [0%, 100%] with a default value as 95%. So the transmission is obtained as

$$t = 1 - \omega\frac{D}{A}\,. \tag{6}$$

The transmission computed this way suffers from resolution problems since the dark channel describes a neighborhood, so does transmission *t*. However, at object boundaries the depth value and consequently the transmission can change abruptly, so the edges of the transmission map must be corrected. For this, a guided filter is implemented that corrects the transmission map using the second derivative of the original image. We use two different guided filter implementations here depending on the size of the filtering kernel because of performance considerations. The first one uses on-the-fly box filtering, the second uses integral images aka Summed Area Tables or (SATs). The second derivatives are computed by the following formula:

$$\begin{aligned} I_{\mathrm{grad2}}[x,y] = \quad & |I[x+1,y] - 2I[x,y] + I[x-1,y]| + \\ & |I[x,y+1] - 2I[x,y] + I[x,y-1]|\,, \end{aligned} \tag{7}$$

where *x* and *y* represent the image coordinates.

2.1.4. Recovering the original image

Having obtained the refined transmission with guided filtering, the final image is recovered. If the original radiance is *L*, then we would see *I* through haze of airlight *A* and transmission *t*:

$$I = tL + (1 - t)A \ . \tag{8}$$

From this, original intensity *L* is

$$L = A + \frac{I-A}{t}. \tag{9}$$

Eq.(9) is numerically unstable for small transmission values *t*, therefore, we limit it with a t_{min} minimum value, which also limits the power of recoverability. Its reciprocal is called amplification and is 20 for 16 bit images and 10 for 8 bit images by default.

Additionally, only for the floating point implementation, the limited transmission is exponentiated differently on the three color channels to compensate the bluish scattering of air. The exponents are *1+3r* on red, *1+2r* on green, and *1+r* on blue, where *r* is the blue removal parameter.

2.2. Deep learning based approach

With recent advancements and success of neural networks and deep learning in multiple fields, it is reasonable to try to use them for dehazing (*Yang et al*., 2018; *Song et al*., 2017). In our implementation, the main idea is that instead of an end-to-end network, we are using a transformed atmospheric scattering equation and we incorporate it directly into the model (*Li et al.*, 2017). The network has a standard convolutional structure, and it is relatively small (less than 2000 parameters). The training generally converges with at most 10 epochs. Details of the network can be found in the cited publication. The main problem is obtaining the training data, which we will address in the following section.

3. Training data acquisition

To adequately train the neural network, we need a large amount of training data. The data set should contain image pairs in the form of pictures with and without fog. Collecting a large enough real-life data set is clearly an unrealistic goal. It would be inevitable that the image pairs would have differences, that are unrelated

to the fog, like disappearing objects. It is a much more plausible idea to synthetically generate the images. If we consider that the network's goal is to remove the effect of the fog, and we can properly model its behavior in our simulation, then it is reasonable to expect the trained network to also work on real-life images as well.

We used the Sponza scene with an artificially added inhomogeneous fog to generate 10.000 images (with 800×600 pixels resolution). The images were stored in a 16-bit format motivated by the discussion in *Section 2.1*. We will examine the algorithm behind the fog simulation and visualization in *Section 3.1*.

This is not the case with satellite images which are taken regularly above the same area. They can also be aligned reasonably well with each other based on camera parameters, current time, and position of the satellite. Images are from the Sentinel-2 satellites with a 10m/pixel resolution. We manually selected pairs of aligned images which were taken shortly after each other, so changes to the landscape were minimal at this precision. One was a clear shot without obscuring participating media, while the other had partially transparent clouds. The images were sliced into square tiles of size 256×256 pixels. A pair of training images is shown in *Fig. 1*.

Fig. 1. A pair of images used to train the neural network.

3.1. Fog generation

Our goal is to simulate and visualize fog in a physically correct way. The implemented algorithm is based on the works of *Wronski* (2018). The process can

be broken down into three parts: fog simulation and storage, light propagation and processing, and finally usage during object rendering.

The algorithm accounts for extinction, out-scattering, and in-scattering of light with a single scattering model. It is a volumetric approach, thus it can work with inhomogeneous fog. The basic idea is to use raymarching, where each view ray is sampled throughout the volume. Extinction and out-scattering are calculated by sampling and accumulating the fog, while we can take into account the in-scattering by accumulating the incoming light for each light source. The problem is that for general camera orientations and positions, the ray marching process can be too slow on the GPU.

To mitigate this issue, we are using voxels aligned with the camera frustum. For the first part, we can use a compute shader to write the density of the fog into each voxel. The fog could be modeled by various methods (e.g., a particle system, grid based simulation, etc.), but in our case we simply used an animated simplex noise. In the second part, ray marching must be done. However, because we are using the previously described data structure, we can do it with one compute shader pass, where each invocation works on blocks of pixels instead of individual rays.

Incoming light is simulated by using shadow maps to accumulate light in the voxels (in the first part), and then it is propagated in the second part (while properly accounting for extinction). Multiple scattering could be handled by an iterative algorithm that propagates light in all direction (*Premože et al.*, 2004) inside the volume in a separate pass, but we did not implement this.

In the end, we have a data structure where every voxel stores an approximation of accumulated fog density from the direction of the camera and the in-scattered radiance from nearby light sources (towards the camera). Using the data structure now is simple, because we can use linear filtering to sample it in the fragment shader during object rendering. Reflected radiance is decreased according to the accumulated fog density, while in-scattering is simply added to the final radiance. The results are shown in *Fig 2*.

Fig. 2. A pair of rasterized images: original and a version with fog.

An important observation is that during camera movement, temporal aliasing can occur as the frustum-aligned voxels are moving. To mitigate this, it is important to maximize the utility of the allocated memory. By the nature of the phenomena, voxels that are close to the observer has larger effect on the results than those that are further away. By using a denser resolution closer to the camera, we can improve the visuals of the fog. Thus, we used an exponential depth distribution instead of a linear one.

The algorithm does not account for blocking geometry, so in certain scenarios fog and light bleeding can occur. This could be addressed by a kind of adaptive voxelization, but it is unclear, how it would work together with the camera frustum alignment.

4. Results

Our results for synthetic images are shown in *Fig 3*. Here we are showing the trained model beside the dark channel prior approach. We can see that this model can successfully decrease the foggy effect. Colors are recovered, and the bluish tint now appears in the correct place. Compared to this model, the dark channel prior technique removes more haze from the image, but some artifacts are left behind. In the second row, an incorrect lightening occurs on the left part of the image. The borders have some artifacts too, and they also appear in the corners of the geometry. In the beginning we used three channel training data, but this resulted in the image shown in *Fig. 4*. We are still investigating this kind of false coloring artifact. We believe that this was caused by our unbalanced training data. To prevent this, we used only the intensity of the ground truth images during the training. This way the network would not prefer one color over the other.

Fig. 3. From left to right: hazy image, dark channel prior, neural network model, ground truth.

Fig. 4. Results with one channel (left), and with three channels (right) training data.

We also tested these methods on some real-life images. Results are shown in *Fig. 5*. The dark channel prior again has some serious artifacts, generally around edges and on the sky, but it also successfully recovers details that are unseen in the original image. Similarly to the previous comparison, the neural network model decreases the effects of the fog, but now more problems appear. Closer objects, where the fog has no effect, have some serious artifacts like whitening or unnatural tint.

Fig. 5. From left to right: hazy image, dark channel prior, neural network model.

We also trained two separate networks on satellite images. It was the same network discussed earlier, except that one incorporated the atmospheric scattering equation as before (*Network A*), while the other omitted this and followed an end-to-end approach (*Network B*). Results are shown in *Fig. 6*. The difference between *Network A* and *B* is that the latter replaces the fully covered (by clouds) parts of the image with generic background that is similar to the general tone. It also applies a considerable blur. *Network A* keeps the opaque clouds intact but tries to tone down the effect of the transparent ones. Still, these are recognizable in the results. Compared to this, the traditional approach provides a vastly different result. The clouds are more prominent, and many artefacts appear.

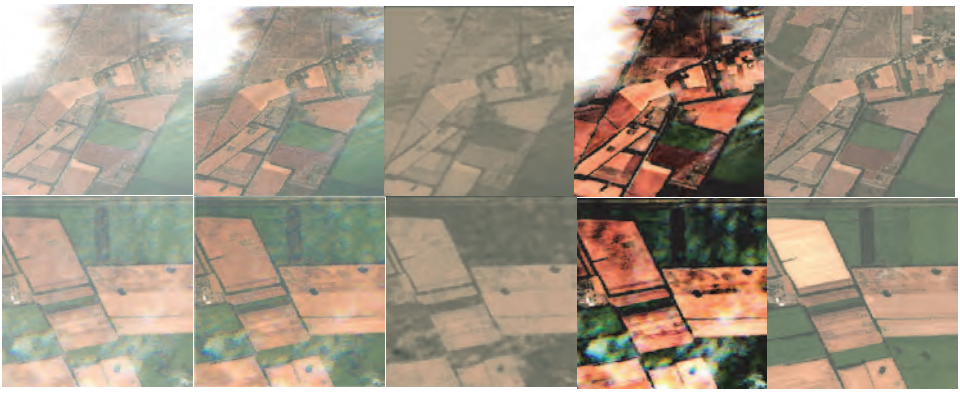

Fig. 6. From left to right: hazy image, Network A, Network B, dark channel prior, ground truth.

5. Conclusion and future work

We have discussed two models for fog removal and a technique for artificial fog rendering. Based on our results, the neural network approach has potential to be used as a dehazing tool, but the variety and balance of the training data is paramount, therefore, we will enhance these aspects for future research. The combination of neural networks and the dark channel prior based method could be also viable, but the performance will likely suffer.

The results on satellite images are promising for the following reasons. An important use-case for these images is to follow the changes in vegetation and in

the landscape. Clouds obscure parts of the image, but generally we have an idea about what we expect to see under them based on previous images of the same area (without clouds). This leads to the following problem: we would like to *predict* the missing parts of the image based on prior information (previous images). It comes naturally to use neural networks to solve this problem, and our results suggest (especially Network B) that a small network can accomplish this with proper additional inputs.

Acknowledgments: The authors would like to express their gratitude towards *Dr. Kálmán Kovács*, *Dr. Dániel Kristóf*, and the *Lechner Knowledge Center* for providing advice and support with the acquisition of satellite images. The research was supported by the Ministry of Innovation and Technology NRDI Office within the framework of the Artificial Intelligence National Laboratory Program. The GPUs have been donated by NVIDIA.

References

He, K., Sun, J. and *Tang, X.*, 2010: Single image haze removal using dark channel prior. *IEEE transactions on pattern analysis and machine intelligence, 33*(12), 2341–2353. https://doi.org/10.1109/CVPRW.2009.5206515

Li, B., Peng, X., Wang, Z., Xu, J., and *Feng, D.*, 2017: Aod-net: All-in-one dehazing network. Proceedings of the IEEE international conference on computer vision, 4770– 4778. https://doi.org/10.1109/ICCV.2017.511

Premože, S., Ashikhmin, M., Tessendorf, J., Ramamoorthi, R., and *Nayar, S.*, 2004: Practical rendering of multiple scattering effects in participating media. Proc. of Eurographics Symposium on Rendering, 2(10.2312):363–374. https://doi.org/10.2312/EGWR/EGSR04/363-374

Song, Y., Li, J., Wang, X., and *Chen, X.*, 2017: Single image dehazing using ranking convolutional neural network. *IEEE Transactions on Multimedia 20*(6), 1548–1560. https://doi.org/10.1109/TMM.2017.2771472

Wronski, B., 2018: Volumetric Fog and Lighting. GPU Pro 360 Guide to Lighting.

Yang, D. and *Sun, J.*, 2018: Proximal dehaze-net: A prior learning-based deep network for single image dehazing. Proceedings of the European Conference on Computer Vision (ECCV), 729–746. https://doi.org/10.1007/978-3-030-01234-2_43

DOI:10.28974/idojaras.2023.4.3

IDŐJÁRÁS

Quarterly Journal of the Hungarian Meteorological Service
Vol. 127, No. 4, October – December, 2023, pp. 459–471

Forecasting critical weather front transitions based on locally measured meteorological data

Mátyás Szántó* and **László Vajta**

Department of Control Engineering and Information Technology
Faculty of Electrical Engineering and Informatics
Budapest University of Technology and Economics
Műegyetem rkp. 3., H-1111 Budapest, Hungary

**Corresponding author E-mail*: mszanto@iit.bme.hu

(Manuscript received in final form September 15, 2023)

Abstract— Certain types of medical meteorological phenomenontransitions can have a significant deteriorating effect on road safety conditions. Hence, a system that is capable of warning road users of the possibility of such conversions can prove to be utterly useful. Vehicles on different levels of automation (i.e., ones equipped with driver assistance systems – DAS) can use this information to adjust their parameters and become more cautious or warn the drivers to be more careful while driving. In this paper, we prove that identifying the critical type of weather front transition (i.e., no front to unstable cold front) is possible based on locally observable meteorological information. We present our method for classifying weather front transitions to non-critical versus critical types. Our developed machine learning model was trained on a dataset covering 10 years of meteorological data in Hungary, and it shows promising results with a recall value of 86%, and an F1-score of 60%.

As the developed method will form the basis of a patent, we are omitting key components and parameters of our solution from this paper.

Key-words: weather front prediction, machine learning, crowdsourcing, local weather and weather fronts, road safety

1. Introduction

In recent years, autonomous vehicle technology has seen an unprecedented scrutiny. However, full self-driving vehicles have still yet to take over the public roads in most parts of the world. The levels of vehicle autonomy is described in *SAE J3016* (2014). On lower levels lie cars with less complex automation features, i.e., driver assistance systems and advanced driver assistance systems. A very important feature of such vehicles is the capability to improve their navigation or at least give instructions to their human drivers – or intervene in some well justifiable cases above level 1 of the six levels of vehicle autonomy.

One key component of driving safety comes from the steady vigilance of the drivers. This ensures that if necessary, the driver is capable of successfully maneuvering unexpected and dangerous road situations. Bad environmental conditions often require the drivers to be more focused. A solution that is capable of warning drivers of the presence of traffic-influencing circumstances are therefore an essential part of modern driving assistance systems, self driving vehicles, and traffic management solutions.

Weather conditions and especially weather front transitions can negatively effect the vigilance of road users, and thus, they are a fundamental consideration for designing such a system. Learning the current (daily) medical meteorological phenomena can currently be accomplished by receiving outputs from expert analyses. This is often not readily available for public use and can be significantly delayed compared to the timing expectations of a low latency traffic management system.

In this paper we present (i) our dataset that was used for training and (ii) a novel machine learning (ML) solution that is capable of yielding suggestions for critical medical meteorological transitions. The paper is constructed as follows: In Section 4.1 we introduce the scientific background of our research. Then in section 2 we present the used datasets and the methods employed in our classification solution. We showcase our results in section 3, then discuss those in section 4 giving an outlook to our future aims in this subject in subsection 4.1.

1.1. Previous work

Weather conditions have a significant direct effect on traffic safety. This is predominantly caused by the effect that precipitation and temperature changes have on visibility and the friction properties of vehicles' tyres and the road surfaces (*Andrey* et al., 2001; *Becker* et al., 2022). Previous research has also argued that medical meteorological conditions also have an indirect negative effect on the frequency of road accidents through negatively influencing humans' vigilance (*Örményi*, 1975).

In our previous work (*Szántó* and *Vajta*, 2019b), we designed a statistical analysis for the inspection of whether this decrease in driver vigilance causes growth in road accidents. For this, we analysed different front transition types in Hungary:

- no front to unstable cold front;
- no front to stable cold front;
- no front to stable warm front;
- no front to unstable warm front;
- unstable cold front to no front;
- stable warm front to no front;
- unstable warm front to unstable cold front;
- stable cold front to unstable cold front.

We successfully showed that there was a significant connection between the transition from no front to unstable cold front, the number of road accidents increased both within and outside city limits in Hungary for the analysed time window, i.e., January 1, 2001–December 31, 2010. In that work, we also proposed an algorithm that allows for information related to medical meteorological phenomenon transitions to be yielded from local meteorological measurements. For this, we proposed a hand-crafted algorithm, whose parameters were tuned empirically in order to effectively suggest a flag that corresponds to the presence of an unstable cold front.

In our previous paper (*Szántó* and *Vajta*, 2019b), we also suggested that such a hazard attribute can be used in an intelligent traffic control system that is capable of warning vehicle operators (autonomous agents or humans) of worsened traffic safety conditions. A framework that is capable of hosting such information is introduced in (*Szántó* and *Vajta*, 2019a). A similar solution is proposed by *Kavas-Torris et al*. (2021), wherein the authors define a system for vehicles connected to a network that offers information of environmental information gathered by an unmanned aerial vehicle (UAV). Among others, the broadcast information includes data on weather fronts.

The usage of ML techniques for the prediction of weather circumstances have seen interest in the last few years (*Singh et al.*, 2019; *Dadhich et al.*, 2021). Binary weather classification problems, such as the one described in this article, have also been studied in depth across the scientific community (*Balamurugan* and *Manojkumar*, 2021). However, to the best of our knowledge, no previous solution focused on the usage ML-based classification of weather front transitions.

2. Data and methods

In this section, we describe the dataset on which our analysis is based, and give an introduction to the methods used during the design of our solution.

2.1. Dataset

As one of the main goals of our research was to find possible connections between local meteorological data and weather front transitions, we used a dataset containing information collected at local meteorological stations in Hungary. The same dataset was previously utilized in *Szántó* and *Vajta* (2019b). For front types, we have obtained medical meteorological phenomena that were recorded on a daily basis for the time period between January 1, 2001 and December 31, 2010. This set of data was supplied by the Data Supply Department of the Hungarian Meteorological Service. The second part of our utilized dataset consists of daily accumulated measurements for selected meteorological observatory sites of the Hungarian Meteorological Service (Budapest, Pécs, Szeged, Debrecen, Szombathely, Győr, Nagykanizsa, and Siófok).

Note that the original local weather dataset that was used in *Vécsei* and *Kovács* (2014) had an hourly resolution, but since we only managed to obtain weather fronts recorded on a daily basis, we accumulated the datapoints. Originally, the local weather dataset contained information for the time period between January 1, 1990 and December 31, 2010. However, for the purpose of the study presented in this paper, we could not make use of measurements taken prior to January 1, 1990, therefore, we cropped the dataset to only contain information starting from this date.

As the feature-set for our ML-based classifier, we used local weather measurements with a few additional derived features. For the previously listed cities, the complete set contains daily average temperature, daily average wind speed, daily average atmospheric pressure, and total precipitation, as well as the variation of the respective values from the previous day. The feature-set also contains one-hot encoded precipitation types for the given days. Additional geographical daily mean temperature differences were calculated between selected city-pairs. Sign of the differences has been decided based on the geographical location of the compared cities. The construction of these features has been described in more depth in our previous paper (*Szántó* and *Vajta*, 2019b).

As our previous results showed, the most critical front transition is from no front to unstable cold front state. Therefore we created a binary target variable whose values relate to this change dynamic:

- The value of 0 (or False) corresponds with no front transition or no critical front transition;
- The value of 1 (or True) corresponds with the critical front transition.

This categorization gave us a strongly unbalanced target variable. The empirical distribution of our target variable is shown in *Fig. 1*.

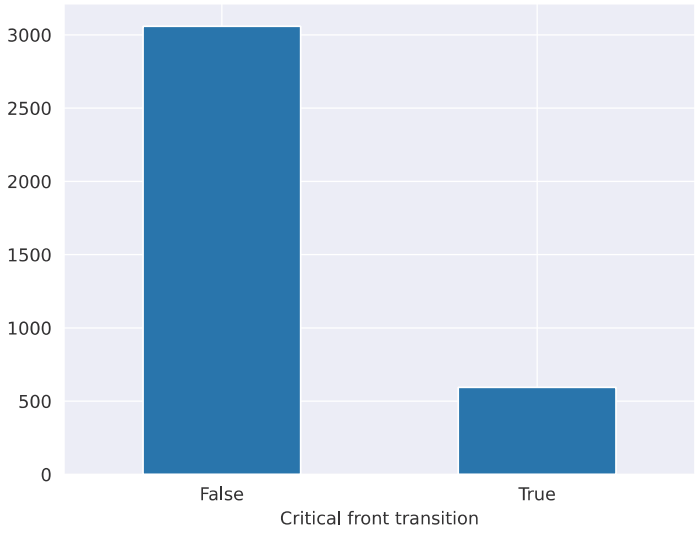

Fig. 1. Heavily unbalanced target distribution. The vertical axis shows the number of transitions. True label denotes critical front transition, while False label denotes no critical front transition.

2.2. Methods

The resulting method presented in this report is used as the basis for a patent filing. Therefore, many steps of the data preprocessing pipeline, as well as the type and parameters of the trained ML algorithm are omitted from this publication.

First, we randomly split the dataset into training and test subsets. We did so using a 90% to 10% ratio. The heavily unbalanced target variable (as shown in *Fig. 1*) made data augmentation a necessity prior to model training. For this purpose, we randomly oversampled and undersampled the respective portions of the training set (*Branco et al.*, 2016). The result of resampling is shown in *Fig. 2*. The distribution of the target variable in the training split following resampling is shown in *Fig. 3*.

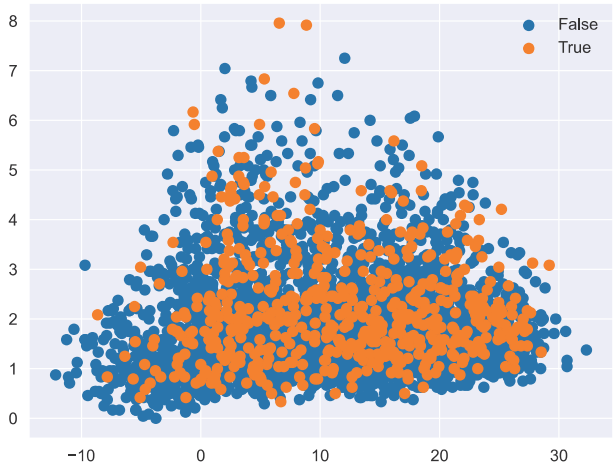

(a)

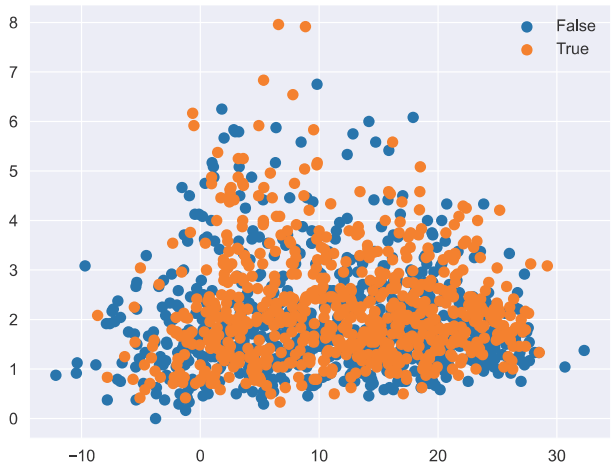

(b)

Fig. 2. Data distribution before (a) and after (b) data augmentation. The vertical and horizontal axes show randomly chosen features. True label denotes critical front transition, while False label denotes no critical front transition.

For binary classification, we used three different approaches:

– a traditional ML technique;
– an Artificial Neural Network-based (ANN) technique; and
– a recently published ML technique that makes use of decision trees and boosting.

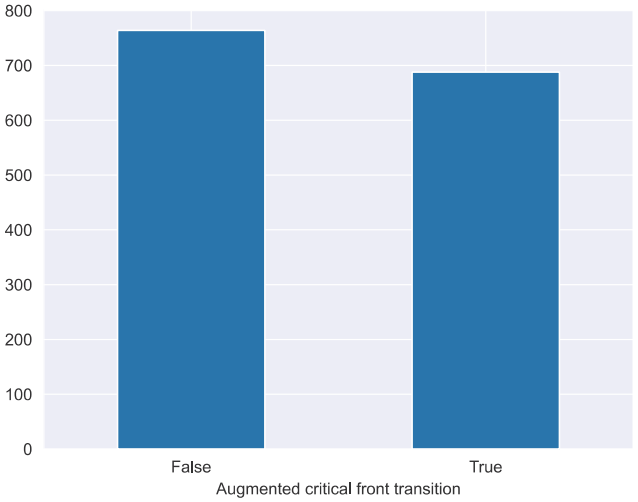

Fig. 3. Augmented training data – target distribution. The vertical axis shows the number of transitions. True label denotes critical front transition, while False label denotes no critical front transition.

In the interest of safeguarding intellectual property rights, technical details are intentionally omitted from this paper, as they constitute foundational aspects of a forthcoming patent application. Therefore, in the following sections of the paper, these will be denoted as Method 1, Method 2, and Method 3.

Method 1 is a decision tree-based multi-class classification ensemble model. The approach used in this paper was proposed in the paper of *Geurts* et al. (2006). We chose this technique, as – similarly to random forest classifiers – it trains multiple decision trees on the training data, but it does not use bagging, and thus, it is less resource-sensitive, while also less prone to overfitting.

For fitting the extra trees classifier, we used the Gini impurity to measure the quality of each split, with minimum 2 samples used to split an internal node. The model was allowed to use at most 12 features to create a split.

We empirically tuned two hyperparameters of the model (number of estimators fitted and minimum number of samples at leaf) as shown in *Table 1*. For comparing the results of the individual models, we used k-fold cross-validation and calculated the test R2 scores.

Method 2 is a fully connected neural network with a depth of 4. It employs dense layers with different activation functions used in the feed forward connections. The simplified structure of the used ANN is shown in *Fig. 4*.

For the hidden layers – l_1 to l_4 in *Fig. 4* – , the rectified linear unit (ReLU) (*Nair* and *Hinton*, 2010) activation function was used, whereas in the case of the final connection – l_4 to l_O in *Fig. 4* –, we employed the softmax function that yields

probability values for the individual output classes. For the outputs of every hidden layer, we used batch normalization. We aided the optimization process with learning rate (LR) scheduling; namely, we used step LR decay, which iteratively applies a division to the learning rate by a prescribed factor (γ) after a given number of epochs pass (S) during training. To help the generalization capability of our network, we used dropout.

Table 1. Parameters used for fitting the Extra Trees model. Best model is shown in bold

Number of estimators	Minimum number of samples at leaf	Mean R^2 test score
1000	20	0.4807
500	20	0.4810
2500	20	0.4813
3000	10	0.4813
3100	**10**	**0.4916**
3125	10	0.4810
3250	10	0.4813
3500	10	0.4804

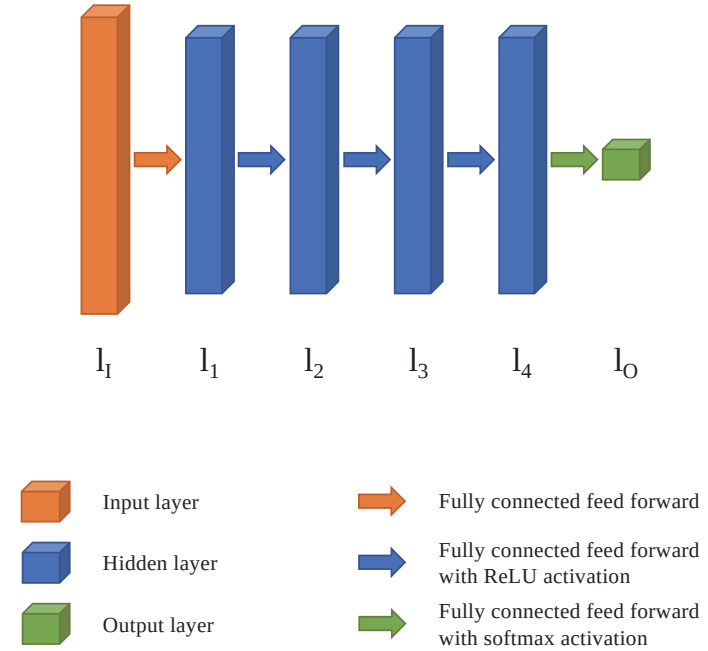

Fig. 4. Simplified structure of our artificial neural network.

We ran random hyperparameter sweeps using the Weights and Biases method (*Biewald et al.*, 2020) finding the optimal hyperparameters for the ANN. We show the individual tuned parameters and the swept ranges in *Table 2*. We trained our network with each parameter-set for 200 epochs using the AdamW optimizer (*Loshchilov* and *Hutter*, 2017), and used the cross entropy loss for training and monitoring the validation performance of the model.

The technical details of **Method 3** are not given here in the interest of guarding intellectual property rights.

Table 2. Parameter tuning of the artificial neural network. l_i denotes the number of nodes in the *i*th layer

Tuned hyperparameter	**Sweep range**		**Optimal value**
	min	**max**	
Batch size	16	2048	256
Learning rate	0.000001	0.01	0.0001
γ	1.5	20	2
S	10	30	15
Dropout	10%	70%	30.58%
l_1	32	512	147
l_2	16	256	151
l_3	8	256	61
l_4	4	128	5

3. Results

We trained the models for all three methods on a server computer with 2 x Nvidia RTX 2080 Super GPUs and an Intel(R) Core (TM) i7-9700K CPU running Ubuntu 22.04. The dataset preparation steps and the training scripts were developed in python using scikit-learn (*Pedregosa et al.*, 2011) and PyTorch (*Paszke et al.*, 2019).

As the aim of the models was to correctly classify the critical front type transition using binary classification, we evaluated and compared the results using

confusion matrices. The no front to unstable cold front transitions are deemed critical, since they cause significant increase of accident numbers. Hence, recall is the most important metric that we want to tune the classifiers for, as this metric indicates the ratio of false negatives (i.e., cases where a critical front transition was observed, but the model missed it and the output showed no critical transition) and all positive cases in the test set. The second most prioritized metric was precision, as this metric shows the ratio of false positives (i.e., the number of cases where no critical front transition was observed, but the model output showed a critical case) and all positive predictions. The results of our training are shown in *Table 3*.

Table 3. Classification results for the trained models. Best results shown in bold

	recall	**precision**	**F1-score**	**training time (seconds)**
Method 1	68.750%	40.367%	50.867%	**0.1697**
Method 2	0.000%	*83.000%*	0.000%	166.7136
Method 3	**85.938%**	**45.833%**	**59.782%**	0.2741

Based on the recall and precision values we clearly identified, that the best candidate model for classifying critical front type transitions based on locally measured meteorological data is Method 3.

This result is also underpinned by the confusion matrices for each method shown in *Fig. 5*.

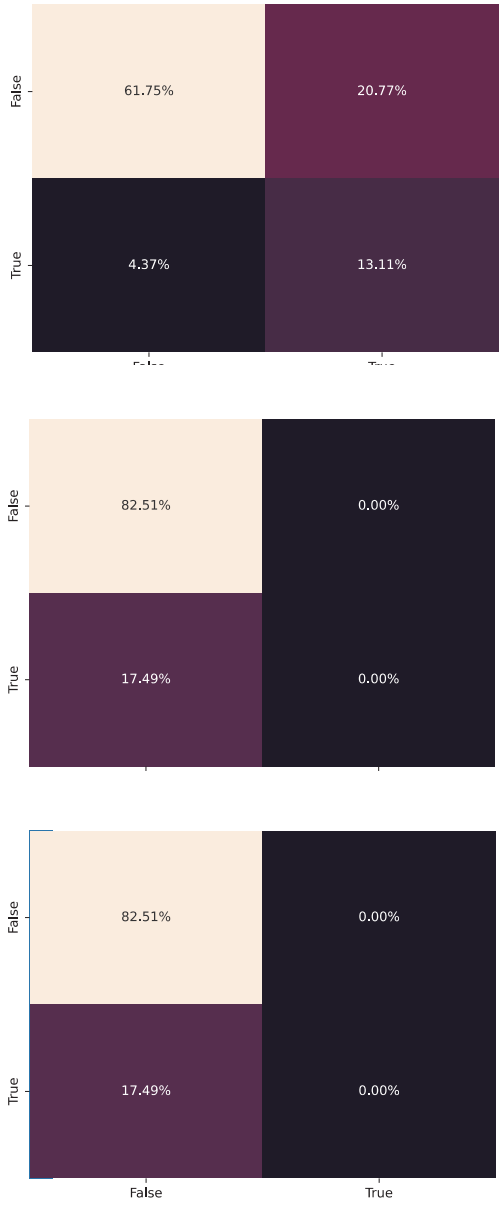

Fig. 5. Confusion matrix of Method 1 (5a), Method 2 (5b), and Method 3 (5c). True label denotes critical front transition, while False label denotes no critical front transition. The horizontal and vertical axes show ground truth values and predicted values, respectively.

4. Discussion

The high precision value observed for Method 2 (83%, shown in italic in *Table 3*) was presumably the result of the unbalanced target distribution of the test set. After further analysis of the predictions given by Method 2, it is obvious that such a high result was caused by the incapability of this method to find and learn the patterns within the training data. We also hypothesize that training that model on a larger dataset would increase its prediction ability.

Moreover, having access to a larger body of input data usually results in the training of any ML-based algorithm less prone to overfitting, i.e., the more diverse the input dataset, the less likely for the model to fit its predictions precisely to the training data. We conjecture, that the lack of ample training data caused all three models to underperform to a varying extent on the test set.

However, given that the most critical front transformation (no front to unstable cold front transition) was labeled as the positive case in the training data, our models were tuned for recall, that is, the main goal was to exhibit the highest possible recall values. An outstanding recall value was achieved by Method 1 and a satisfactory result was observed for Method 3 (see *Table 3*).

4.1. Future work

A key future development goal of our method – as mentioned several times through the previous sections – is to file for a patent and to protect the novelty of our technique.

We would like to test the possible performance gains our methods can exhibit given the availability of a larger amount of training data, as we argue that such an improvement would enable our models to become less prone to overfitting.

Another important opportunity for optimization could arise from more precise data preparation; in the current solution, feature selection for the models was performed heuristically. After that, feature usage was automatically determined by the training algorithms and the models themselves. We hypothesize that the models, more precisely the training processes, would substantially benefit from expert contributions.

Acknowledgments: The authors would like to thank Dr. Kálmán Kovács and the Data Supply Department of the Hungarian Meteorological Service for sharing the extensive local and medical meteorological and accident databases for the purpose of the research presented in this paper. The research presented here was supported by the the European Union project RRF-2.3.1-21-2022-00004 within the framework of the Artificial Intelligence National Laboratory.

References

Andrey, J.C., Mills, B.E., and *Vandermolen, J.,* 2001: Weather information and road safety. Paper Series of the Institute for Catastrophic Loss Reduction Toronto, Ontario, Canada 15.

Balamurugan, M.S. and *Manojkumar, R.,* 2021: Study of short term rain forecasting using machine learning based approach. *Wireless networks 27*, 5429–5434. https://doi.org/10.1007/s11276-019-02168-3

Becker, N., Rust, H.W., and *Ulbrich U.,* 2022: Weather impacts on various types of road crashes: a quantitative analysis using generalized additive models. *Eur. Transport Res. Rev. 14.1*, 1–18. https://doi.org/10.1186/s12544-022-00561-2

Biewald, L., 2020: Experiment tracking with weights and biases. Software available from wandb. com 2, p. 233.

Branco, P., Torgo, L., and *Ribeiro, R.P.,* 2016: A survey of predictive modeling on imbalanced domains. *ACM computing surveys (CSUR) 49*(2), 1–50. https://doi.org/10.1145/2907070

Dadhich, S., Pathak, V., Mittal, R., Doshi, R., 2020: Machine learning for weather forecasting. In (Eds.: *Hiran, K.K., Khazanchi, D., Ajay Kumar Vyas, A.K., Padmanaban, S.*) Machine Learning for Sustainable Development. 161–174. https://doi.org/10.1515/9783110702514-010

Geurts, P., Ernst, D., and Wehenkel, L. 2006: Extremely randomized trees. *Machine learning 63*, 3–42. https://doi.org/10.1007/s10994-006-6226-1

Kavas-Torris, O., Gelbal, Sukru Yaren, Cantas, Mustafa Ridvan, Guvenc, Bilin Aksun, and Guvenc, L., 2021: Connected UAV and CAV Coordination for Improved Road Network Safety and Mobility. Tech. rep. SAE Technical Paper. https://doi.org/10.4271/2021-01-0173

Loshchilov, I. and *Hutter, F.,* 2017: Decoupled weight decay regularization. arXiv preprint arXiv:1711.05101.

Nair, V. and *Hinton, G.E.,* 2010: Rectified linear units improve restricted boltzmann machines. Proceedings of the 27th international conference on machine learning (ICML-10), 807–814.

Örményi, I., 1975. Érzékenyek vagyunk. *Heves Megyei Népújság 26*.9. (In Hungarian)

Paszke, A., Gross, S., Massa, F., Lerer, A., Bradbury, J., Chanan, G., Killeen, T., Lin, Z., Gimelshein, N., and Antiga, L., 2019: Pytorch: An imperative style, high-performance deep learning library. In: Advances in neural information processing systems 32.

Pedregosa, F., Varoquaux, G., Gramfort, A., Michel, V., Thirion, B., Grisel, O., Blondel, M., Prettenhofer, P., Weiss, R., Dubourg, V., Vanderplas, J., Passos, A., Cournapeau, D., Brucher, M., Perrot, M., and Duchesnay, E., 2011: Scikit-learn: Machine Learning in Python. *J. Mach. Learn. Res. 12*, 2825–2830.

Singh, N., Chaturvedi, S., and *Akhter, S.,* 2019: Weather Forecasting Using Machine Learning Algorithm. 2019 International Conference on Signal Processing and Communication (ICSC), pp. 171–174. https://doi.org/10.1109/ICSC45622.2019.8938211

Szántó, M. and *Vajta, L.,* 2019a: Introducing CrowdMapping: A Novel System for Generating Autonomous Driving Aiding Traffic Network Databases. 2019 International Conference on Control, Artificial Intelligence, Robotics & Optimization (ICCAIRO), 7–12. https://doi.org/10.1109/ICCAIRO47923.2019.00010

Szántó, M. and *Vajta, L.,* 2019b: Towards an intelligent traffic control system using crowdsourcing, based on combined evaluation of weather information and accident statistics. *Időjárás 123*, 295–312. https://doi.org/10.28974/idojaras.2019.3.3

SAE J3016, 2014: Taxonomy and Definitions for Terms Related to Driving Automation Systems for On-Road Motor Vehicles. SAE Standard J3016, Rev. Apr. 2021.

Vécsei, P. and *Kovács, K.,* 2014: Statistical analysis of relationships between road accidents involving personal injury and meteorological variables in Hungary. *Időjárás 118*, 349–378.

DOI:10.28974/idojaras.2023.4.4

IDŐJÁRÁS

Quarterly Journal of the Hungarian Meteorological Service
Vol. 127, No. 4, October – December, 2023, pp. 473–484

A comparison of river streamflow measurement from optical and passive microwave radiometry

Zsófia Kugler * and **Viktor Győző Horváth**

Department of Photogrammetry and Geoinformatics
Budapest University of Technology and Economics
Műegyetem rkp. 3, H-1111 Budapest, Hungary

**Corresponding author E-mail kugler.zsofia@emk.bme.hu*

(Manuscript received in final form September 15, 2023)

Abstract— Climate change has a crucial impact on the global energy and water cycle. The hydrological cycle can be studied both from ground and satellite measurements on a global scale. Yet a comprehensive overview is challenging to establish given the spatial and temporal limitations related to various Earth Observation satellite sensors or maintenance of in-situ gauges. Optical remote sensing of visible light can not overcome the substantial obstacle from cloud cover that vastly limits its capability in daily global monitoring. Active satellite sensors like SAR or altimetry are not capable to provide global coverage on a daily basis, therefore, they can be geographically limited. Passive microwave radiometry (PMR) can acquire both daily and global scales that enables the temporally frequent and spatially extensive observations of continental river gauge. Previous studies demonstrated the use of PMR measurements for global daily river gauge benefiting from its high sensitivity of microwave radiation to water presence. This study aims at comparing the methodology of PMR to optical river gauge measurements based on the assumption that at selected locations along the river channel, increase in streamflow is related to increase in the floodplain water surface inundation. Comparison showed a significant obstacle of cloud cover over tropical regions, where PMR has the potential to measure river streamflow. Yet over regions with less clouds both optical and PMR can be good alternative to in-situ streamflow ground measurements.

Key-words: passive microwave radiometry, optical remote sensing, space hydrology, climate change impact, river gauge

1. Introduction

Climate change is impacting our everyday life and alters the magnitude and frequency of extreme weather related events such as precipitation, floods, and drought.

The Moderate Resolution Imaging Spectroradiometer (MODIS), a low resolution (250 m – 5 km) NASA satellite is playing a key contribution in applications that require frequent, large-scale observations such as streamflow monitoring. The two platforms, carrying MODIS sensor on-board, Aqua (launched in 2002) and Terra (launched in 1999) are monitoring the Earth every day with an almost full coverage of its complete surface for more than two decades. The unique collection of MODIS data for this reason enables long term monitoring of environmental phenomena and variations or trends in their behavior. It has the significant potential to capture river flow variations and assess global trends with the use of extended time series stretching over decades. Data can be obtained on no charge basis from different services like the https://modis.gsfc.nasa.gov/data/ that collects and provides data on different productions levels and applications like land, cryosphere, and oceans. MODIS is also provided on a near-real time basis at https://worldview.earthdata.nasa.gov/ just within 3–5 hours of being observed enabling rapid response to different types of natural or man-made disasters.

For all the above advantages, MODIS is playing a unique contribution to map physical processes of the Earth, especially to monitor the evolution of river streamflow on an almost daily frequency. Therefore, numerous applications have flourished in the past using MODIS images to observe rivers (*Brakenridge* 2005, *Zhan et al*, 2002; *Thenkabail*, 2005; *Sakamoto*, 2007; *Tarpanelli*, 2020). Still to overcome significant limitations related to cloud cover, the use of microwave emission of the Earth's surface measured by passive microwave satellite radiometers (PMR) has a notable contribution to continental streamflow measurement as demonstrated in several previous publications (*Brakenridge*, 2007, 2023; *Kugler et al.*, 2019)

In the past, we used both satellite Ka- (36.5 GHz) and L-band (1-2 GHz) passive microwave radiometry (PMR) data to acquire river discharge around the globe on a near-daily basis. Methodology is even capable of monitoring arctic river ice break-up during spring and freeze-up in the autumn allowing to understand climate change related internal variations of ice phenology at high latitudes (*Podkowa*, 2023).

2. Methodology

2.1. Passive microwave radiometers

The aim of using PMR in streamflow observations is the long-term, systematic monitoring of rivers across the world. The method was initially developed for Ka-band AMSR-E passive microwave senor data. The observations of the descending orbit, H polarization, and 36 GHz frequency, were found to be sensitive to water surface changes. In further studies we extended our investigations to low frequency PMR like ESA SMOS and NASA SMAP (2 GHz) sensors due to its better performance on tropical humid climate (*Kugler*, 2019). Brightness temperature (*Tb*) measured by a passive microwave radiometer is related to the physical temperature (T) and the emissivity (ε) of the surface given by:

$$Tb = \varepsilon\, T. \tag{1}$$

In general, a lower $Tb(m)$ occurs over a footprint containing water bodies compared to a higher $Tb(c)$ over a footprint on land without surface water. Under a constant physical temperature T, $Tb(m)$ decreases over locations along river channel, where rising water level (river stage) causes a corresponding increase in the water surface extent. However, microwave radiation is also influenced by many factors including physical temperature (T), permittivity (P), surface roughness (R), and soil moisture (θ):

$$Tb = \mathrm{f}\,(T, P, R, \theta)\ . \tag{2}$$

Information related to surface water change is primarily conveyed in the emissivity controlled by the effective permittivity over the targeted area, while other factors such as roughness, soil moisture, vegetation cover, and atmospheric conditions may affect the brightness temperature as measured by an orbiting satellite radiometer above the atmosphere. According to Eq.(1), the physical temperature T must be cancelled out in order to get at the emissivity ε. This is achieved approximately by taking the measurement $Tb(m)$ value received over a river channel (measurement pixel) as the denominator with the numerator being a calibration observation $Tb(c)$ not influenced by water change (calibration pixel), which is chosen in the vicinity of the measurement pixel so that the physical temperature T is similar thanks to the long correlation length of regional temperature variability. In this method, the signal ratio is defined by the relationship:

$$C/M\ Ratio = Tb(c)/Tb(m) \sim T\,\varepsilon(c)/\,[T\,\varepsilon(m)] = \varepsilon(c)/\varepsilon(m)\ , \tag{3}$$

where *Tb*(*c*) and *Tb*(*m*) are the brightness temperature of the calibration and measurement pixel, respectively.

The time series of the extracted *C/M* Ratio results in systematic satellite based hydrograph measurements for selected river reaches with a daily or near-daily temporal resolution. With this satellite method, the detection of flow condition changes over ungauged and inaccessible remote river channels is, in principle, feasible from space on a frequent temporal sampling. To compare PMR technics to optical low resolution data, we selected 22 satellite river gauges (SGR) over various river basins around the world from a PMR database of 2000 monitored SGRs (*Fig. 1*), over which PMR was proved to be in good agreement with ground measurements (*Kugler*, 2019). Data was compared for a time series from 2010 to present.

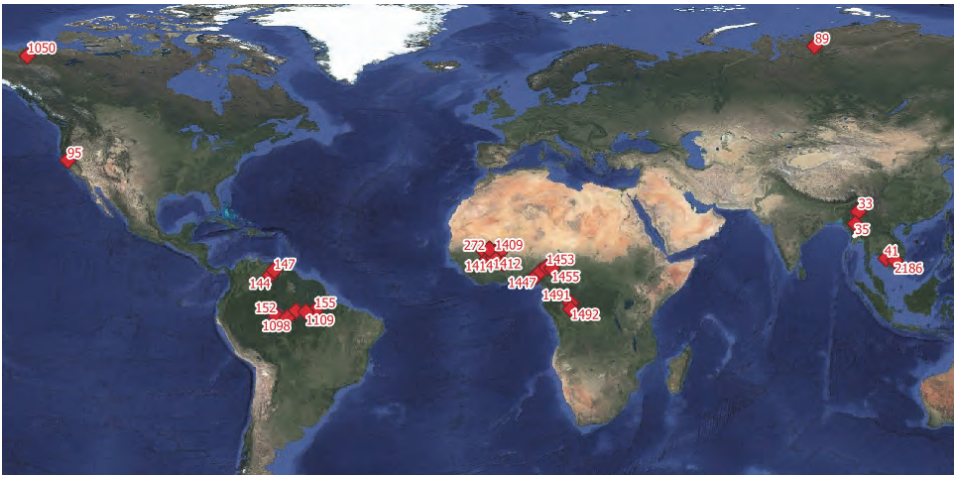

Fig. 1. Map of river gauging sites around the globe obtained from both PMR and optical data.

2.2. Optical MODIS data from Google Earth Engine

To compare PMR streamflow observations to MODIS river gauge, we use Google Earth Engine (GEE) to analyze considerable amount of optical satellite time series. Calculations were carried out on the Google Earth Engine Code Editor, a web-based integrated development platform (IDE) for the GEE JavaScript Application Programming Interface (API) (*Fig. 2*). GEE is an online cloud computing platform for processing multispectral and SAR satellite imagery. GEE

was launched in 2010, and its datasets have been continuously expanded ever since. GEE is a free of charge web-based tool for academic purposes, where commercial use has recently been limited. GEE provides both Python and JavaScript APIs to the petabyte size Earth Observation (EO) satellite dataset of several decades. GEE Code Editor offers a Google Maps-based data visualizer capable to store and analyze satellite data. Numerous data sources can be instantly accessed and processed using GEE, which is very convenient for global or time related remote sensing studies (*Gorelick* 2017).

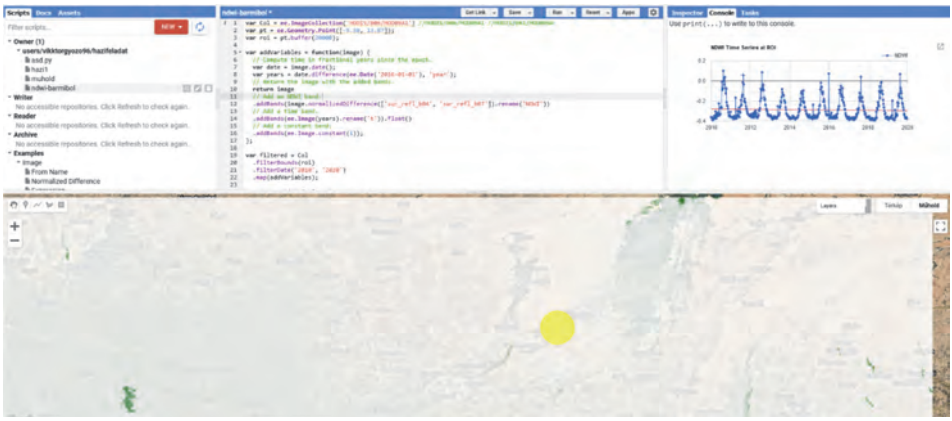

Fig. 2. Google Earth Engine Code Editor IDE capable to analyze several decades of Earth Observation satellite data. Yellow circle marks the extent of the 20 km buffer around SGR to select MODIS observations for streamflow analysis.

For comparison with PMR streamflow observations, we analyzed the MOD09A1.061 Terra Surface Reflectance 8-Day Global 500m dataset. This is a pre-processed dataset from data recorded by the MODIS (Moderate Resolution Imaging Spectroradiometer) sensor on the Terra satellite, which was launched in 1999. At the time of writing data can be accessed in the February 18, 2000 – July 4, 2023 time interval from this dataset. Terra-MODIS instruments scan the entire Earth's surface every 1 to 2 days. Terra MOD09A1 Version 6.1 product used in this study provides an estimate of the surface spectral reflectance of Terra MODIS Bands 1 through 7 corrected for atmospheric conditions such as gases, aerosols, and Rayleigh scattering. For each pixel, a value is selected from all the acquisitions within the 8-day composite period. The criteria for the pixel choice include cloud and solar zenith. When several acquisitions meet the criteria, the pixel with the minimum channel 3 (blue) value is used.
(https://developers.google.com/earth-engine/datasets/catalog/MODIS_061_MOD09A1)

The dataset used in the analysis has a spatial resolution of 500 meters with the following bands and spectral resolutions:

sur_refl_b01	620–670 nm
sur_refl_b02	841–876 nm
sur_refl_b03	459–479 nm
sur_refl_b04	545–565 nm
sur_refl_b05	1230–1250 nm
sur_refl_b06	1628–1652 nm
sur_refl_b07	2105–2155 nm

To resemble the methodology of PMR observing water surface changes within the footprint of the microwave observations, we calculated NDWI for each MODIS pixel. For the NDWI calculations, the 4th band (545–565nm) and the 7th band (2105-2155nm) were used, with the standard formula of:

$$NDWI = \frac{(sur\_refl\_b04 - sur\_refl\_b07)}{(sur\_refl\_b04 + sur\_refl\_b07)}. \quad (4)$$

Because of the low spatial resolution of MODIS, data was aggregating neighboring pixels around the predefined locations of the selected 22 PMR SGR. Around each selected SGR location, a circular buffer of 20 km was applied, and NDWI values for each calculated pixel within the area are aggregated (*Fig. 3*). Calculations and display for one point took around 470 secs in GEE for the time series 2010–2022, but from this around 400 is displaying the calculated mosaics. Generating time series plots of any SGR took 10 seconds for 10 years of data. There was no filtering based on quality metrics provided for individual MODIS scenes (e.g., cloudy weather).

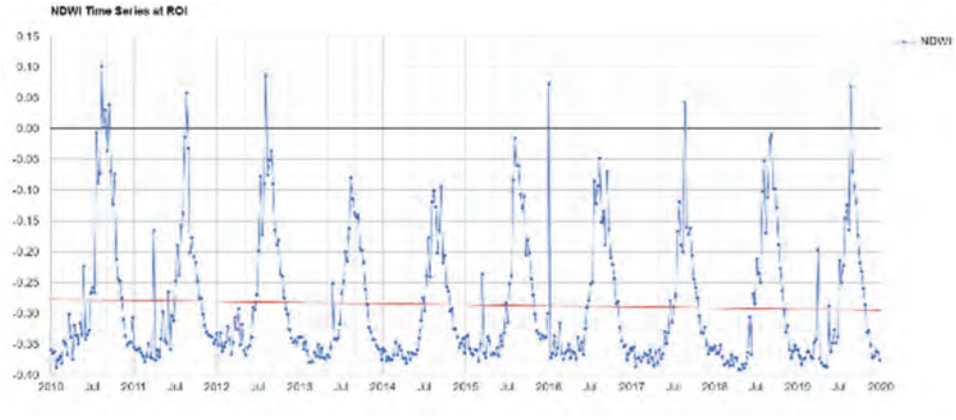

Fig. 3. A dataset derived in the 2010-2020 range for the SGR 64 over the Niger River, in Nigeria.

The time series were then automatically converted to a CSV format so they could be compared with previous PMR data analyzed in MATLAB environment. The script has been run for 22 SGR sites, and then compared to PMR streamflow observations from SMOS time series (2010–2022).

3. Results

The satellite river gauge observation from optical MODIS and PMR SMOS data show similar pattern in time (*Fig. 4*). As on the example of the Irrawaddy River in Myanmar SGR 35 (22.13°N, 96.03°E), both SMOS and MODIS follow the annual periodicity of the streamflow with high-flow state during summer and low-flow state during winter. Both time series follow the annual variation of humid tropical climate dominated by monsoon precipitation between May and October. In-situ data collected at Mandaly gauging station in Myanmar reflects high correlation between satellite and ground streamflow measurement regardless of the optical or PMR dataset (*Fig. 4*). Both dataset are in a high correlation as shown on the scatterplot. Results underline the robustness of the methodology observing water surface area change as an indicator for streamflow variation from both optical and microwave radiometers.

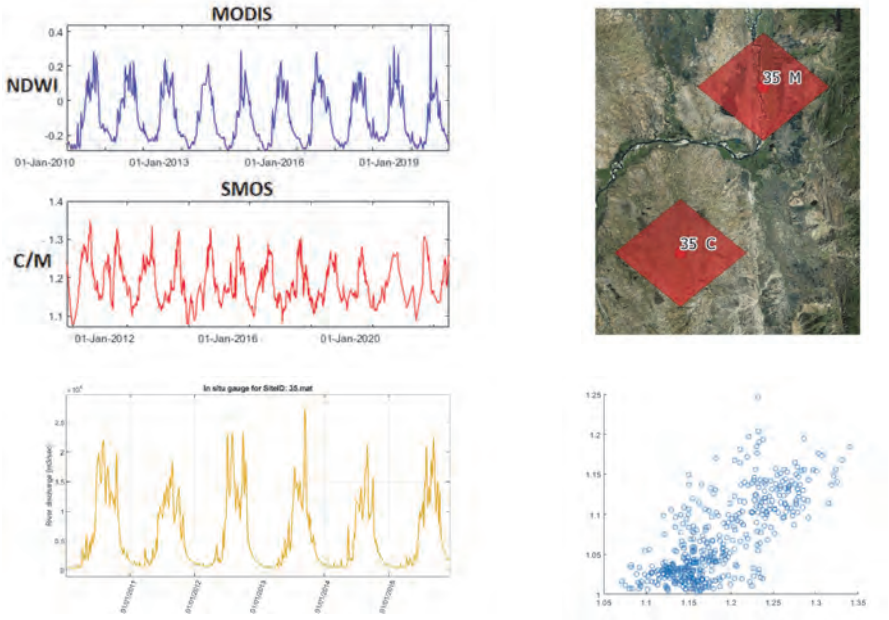

Fig. 4. Satellite river gauge derived from MODIS optical imagery (upper left) and SMOS PMR data (upper right) for SGR 35 (22.13°N, 96.03°E) over the Irrawaddy River in Myanmar. Map shows the location of PMR SGR for both M and C observation (upper right). Lower left figure shows in-situ streamflow [in m/s^2 units] data for the same period (lower left). Lower right figure is a scatterplot of SMOS and MODIS orbital gauge data.

In Ghana, over the White Volta basin, which is the largest rivers sub-basin of the Volta River in West Africa, SGR 1424 shows similar time series pattern for both SMOS and MODIS observations (*Fig. 5*). Tropical humid climate with wet summer (May–October) with southwest winds originating over the Atlantic Ocean and dry winter with strong dry warm winds from the desert in north cause an annual high-flow in summer and low-flow during winter. Most precipitation occurs in August, whereas the streamflow usually peaks in September.

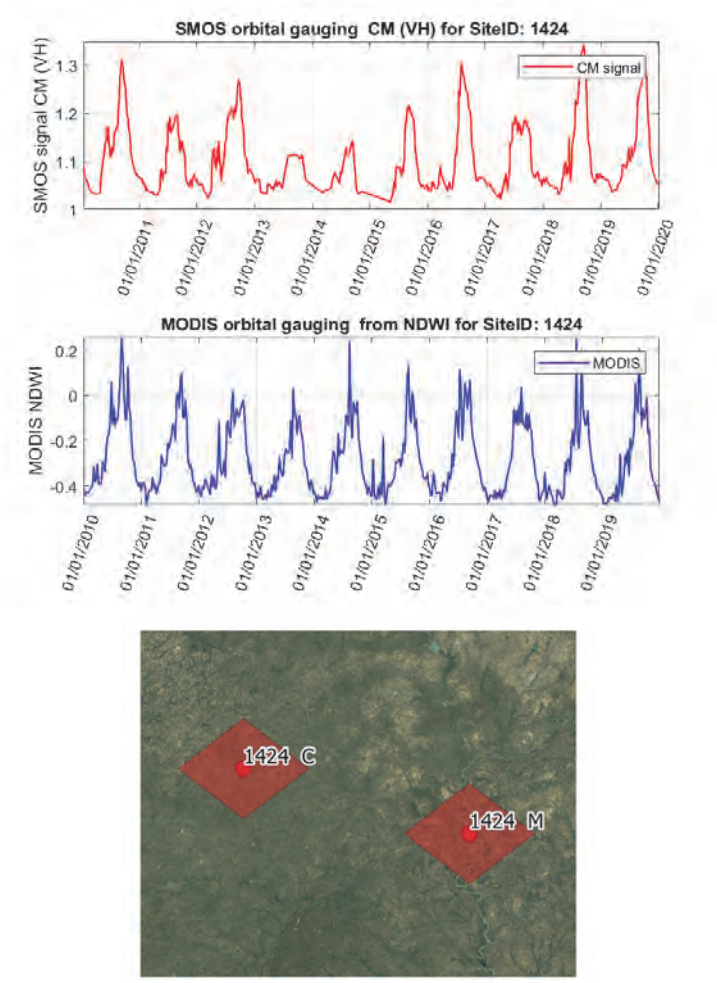

Fig. 5. Satellite river gauge derived from MODIS optical imagery and SMOS PMR data (upper two plots) for SGR 1424 (10.28°N, 1.05°W) over the White Volta River in Ghana. Lower map shows the location of PMR SGR for both M and C observation.

For SGR 1424 SMOS observation exhibits less noise than the MODIS observation. The number of observations is more than twice as many as for the optical data, but it is not the reason for higher noise. On the other hand, the channel width at the satellite gauging location is about 80 m, which is a relatively narrow river channel to measure discharge from space. That concludes that despite low resolution of SMOS, the sensitivity of water surface presence in the footprint enables the observation of inundation increase even for relatively low proportion of water within the observation (narrow river channel). It emphasises the strong capability of microwave emission to measure streamflow from space using all weather satellite systems on a near-daily basis with PMR data. Regarding optical data, given its strong limitation to cloud cover, it can only obtain information over regions, where cloud free scenes can be acquired within frequent time intervals.

The latter requirement is difficult to meet in wet tropical regions with strong cloud cover hindering the acquisition of optical data. As an example over the Purus River, a large tributary of the Amazon River in Brazil (*Fig. 6*), MODIS exhibits a high noise when compared to SMOS with clear seasonal variability of streamflow well correlating with ground gauge (*Kugler,* 2019). Comparing the two different measurements in a scatterplot confirm the low agreement of the MODIS and SMOS, as it can be seen on the scatterplot in the lower left figure. The reason for that might be cloudcover or the very complex environment that does not allow to accurately map inundation from optical data. The reason for more noise in the optical data needs further investigation. Yet the measurement of wet tropical climate seems to support the assumption that cloud cover may be a major limitation factor in near-daily observations.

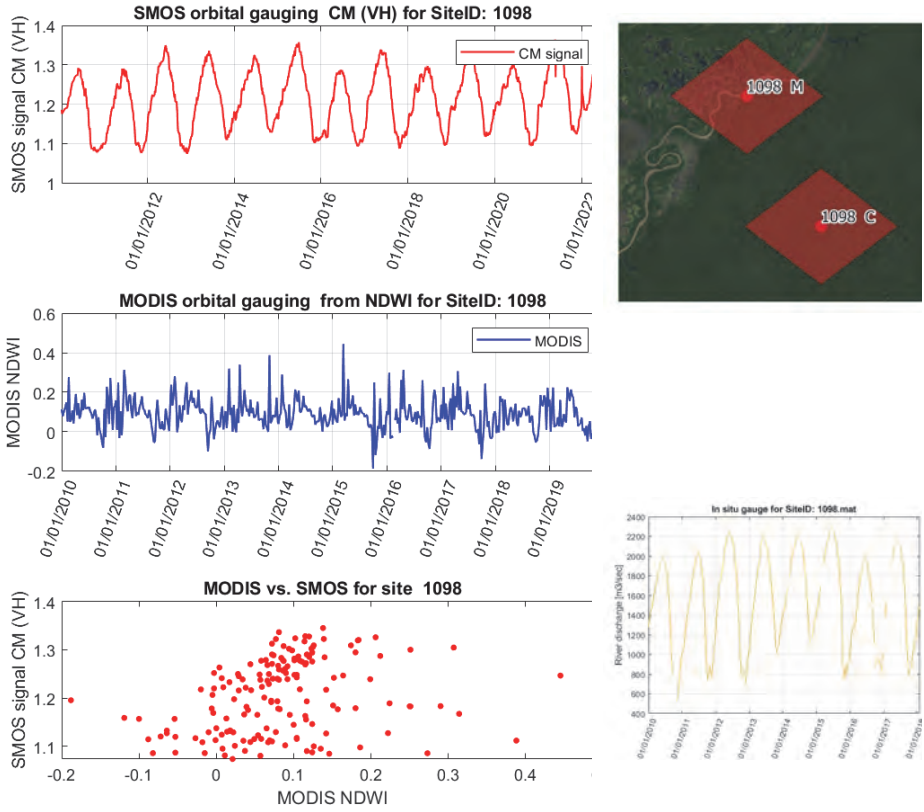

Fig. 6. Satellite river gauge derived from MODIS optical imagery and SMOS PMR data for SGR 1098 (4.65°S, 61.59°W) over the Purus River in Brazil (upper two figures). Upper right map shows the location of PMR SGR for both M and C observation. Lower right figure plots in-situ streamflow data [in m^3/s units]. Lower left graph is a scatterplot of SMOS and MODIS orbital gauge data.

4. Conclusions

This paper demonstrated the use of optical and PMR satellite technologies for continental river streamflow measurement. Satellite data were measuring river gauge from space using the strong correlation between water surface inundation and discharge over selected river reaches. Both optical and microwave satellite data were proved to be suitable for streamflow measurement.

Selected examples of orbital gauges suggest that cloud cover is a significant limitation for optical data. Yet some tropical climate showed good agreement between validated SMOS streamflow data and MODIS gauge time series despite high probability of clouds (like the example over the Irrawaddy or the Volta River). Dense tropical forest is also decreasing the accuracy of optical data reducing its capability to measure water extent over dense vegetation, as it is demonstrated on the example of the Amazon River basin.

Knowing that global climate change is expected to increase the magnitude and frequency of natural hazards like floods; it is crucial to understand changes in the terrestrial water cycle to face future challenges of climate change. Results could be used over ungauged river sections to check validity and double confirm results of PMR river gauge by independent measurements like optical data. It would be important over watersheds, where no validation data can be acquired, or hydrologic data is not collected or shared among major stakeholders. Thus, the comparison of results from both optical and PMR methods would be important to obtain reliable gauging time series from space without the need of collecting ground truth for validity.

Acknowledgement: Part of the work presented was supported by the National Research and Innovation Office.

References

Brakenridge, G.R., Anderson, E., 2005: MODIS-based flood detection, mapping, and measurement: the potential for operational hydrological applications. In: J., Marselek, G., Stacnalie, G., Bálint (eds.): Transboundary Floods, reducing risks through flood management NATO Science Series, *IV Earth and Environmental Scineces Vol. 72,* Springes, The Netherlands, 1-12.

Brakenridge, G.R., Nghiem, S.V., Anderson, E., Mic, R., 2007: Orbital microwave measurement of river discharge and ice status, *Water Resour. Res. 43*, W04405. https://doi.org/10.1029/2006WR005238

Brakenridge, G.R., Nghiem, S.V., and *Kugler, Z.*, 2023: Passive microwave radiometry at different frequency bands for river discharge retrievals. *Earth Space Sci. 10*, e2023EA002859. https://doi.org/10.1029/2023EA002859

Gorelick, N., Hancher, M., Dixon, M., Ilyushchenko, S., Thau, D., Moore, R., 2017*:* Google Earth Engine: Planetary-scale geospatial analysis for everyone, *Remote Sensing of Environment* Volume 202, 1 December 2017, Pages 18-27 doi:10.1016/j.rse.2017.06.031

Kugler, Z., Nghiem, S.V., and Brakenridge, G.R., 2019: L-Band Passive Microwave Data from SMOS for River Gauging Observations in Tropical Climates *Remote Sens. 11*, 835. https://doi.org/10.3390/rs11070835

MOD09A1.061 Terra Surface Reflectance 8-Day Global 500m dataset
https://developers.google.com/earth-engine/datasets/catalog/MODIS_061_MOD09A1#bands

Podkowa, A., Kugler, Z., Nghiem, S.V., and *Brakenridge, G.R.*, 2023: Ice freeze-up and break-up in Arctic Rivers Observed with satellite L-band passive microwave data from 2010 to 2020. *Water Resour. Res.* 59, e2022WR031939. https://doi.org/10.1029/2022WR031939

Sakamoto, T., Nguyen, N. V., Kotera, A., Ohno, H., Ishitsuka, N., and Yokozawa, M., 2007: Detecting temporal changes in the extent of annual flooding within the Cambodia and the Vietnamese Mekong Delta from MODIS time-series imagery. *Remote Sensing of Environment, 109(3),* 295-313.

Tarpanelli, A., Iodice, F., Brocca, L., Restano, M., and *Benveniste, J.*, 2020*:* River Flow Monitoring by Sentinel-3 OLCI and MODIS: Comparison and Combination. *Remote Sens. 12*, 3867. https://doi.org/10.3390/rs12233867

Thenkabail, P.S., Schull, M., and *Turral, H.*, 2005: Ganges and Indus river basin land use/land cover (LULC) and irrigated area mapping using continuous streams of MODIS data. *Remote Sens. Environ. 95*, 317–341. https://doi.org/10.1016/j.rse.2004.12.018

Zhan, X., Sohlberg, R.A., Townshend, J.R.G., DiMiceli, C., Carroll, M.L., and *Eastman, J.C.*, 2002: Detection of land cover change using MODIS 250 m data. *Remote Sens. Environ. 83*, 336–350. https://doi.org/10.1016/S0034-4257(02)00081-0

DOI:10.28974/idojaras.2023.4.5

IDŐJÁRÁS

Quarterly Journal of the Hungarian Meteorological Service
Vol. 127, No. 4, October – December, 2023, pp. 485–504

Climate change in the Debrecen area in the last 50 years and its impact on maize production

Béla Gombos[1,2,*] , **Zoltán Nagy**[1], **András Hajdu**[3], and **János Nagy**[1]

[1]*Institute of Land Use, Engineering and Precision Farming Technology*
Faculty of Agricultural and Food Sciences and Environmental Management
University of Debrecen
Böszörményi út 138., Debrecen, H-4032, Hungary

[2]*Department of Irrigation and Land Improvement*
Institute of Environmental Sciences
Hungarian University of Agriculture and Life Sciences
Szabadság út 1-3., Szarvas, H-5540, Hungary

[3]*Faculty of Informatics, University of Debrecen*
Kassai út 26., Debrecen, H-4028, Hungary

**Corresponding author E-mail: gombos.bela@uni-mate.hu*

(Manuscript received in final form August 23, 2023)

Abstract— The average yield of maize is significantly dependent on the meteorological conditions of the growing year. Both the most favorable weather conditions and the weather anomalies that tend to cause damage depend on the given phenophase. The aim of this research is to analyze the climatic changes that are important in maize production in the Hajdúság region.

For the climatological study of the area, homogenized temperature and precipitation data from the Hungarian Meteorological Service was used for the Debrecen region, which are freely available for download from the data repository of the institution. Trend analysis was performed for the last 50-year (1973–2022) and 30-year (1993–2022) periods. In total, 40 meteorological data series matching the study objective were analyzed. Linear regression calculations were performed using the SPSS 27 statistical software. For the non-parametric procedure, the MAKESENS Excel application was used, based on the Mann-Kendall (MK) test and Sen's slope estimation.

This research shows that the choice of the length of the study period affects the results of trend analysis. The numerical values of the trend slope for the 30-year vs. 50-year period differ, and for some parameters there are also substantial differences (e.g., trend sign). The results of the parametric and non-parametric trend analyses differed only marginally for the

temperature variables included. Also, for precipitation data that do not follow a normal distribution (e.g., monthly), there were only a few significant differences. The trend in mean annual temperature shows an increase of 0.39 and 0.52 °C in 10 years, and an increase of around 2 °C in 50 years and 1.5 °C in 30 years. There is a significant warming in both the summer and winter half-years, with the summer half-year showing a steeper upward trend in the 50-year data series and the winter half-year in the 30-year data series. There is a clear pattern of large, highly significant warming in the summer months and less significant changes in the two spring and two autumn months that were observed. A negative, non-significant trend in annual precipitation is observed. The decreases of 17 mm and 24 mm/10 years obtained for the 50- and 30-year time series are not negligible from a practical point of view. For the summer half-year, the precipitation amount is decreasing, with a slope of -27 mm/10 years for the last 30 years, but even this value is not significant due to the high variability. There is no significant change in the amount of precipitation in the winter half-year over the last decades. Significant trends cannot be detected from monthly or even semi-annual or annual precipitation data. The Mann-Kendall test showed a trend decrease only in the 30-year April data series at the p=0.1 significance level. Overall, the changes are negative for maize production. It should be highlighted that the obvious warming, combined with a slight decrease in precipitation, is leading to a deterioration in crop water availability and a reduction in crop yields. The impact of the identified adverse climatic changes can be compensated to a significant extent by the proposed agrotechnical responses.

Key-words: temperature, precipitation, trend, Mann-Kendall test, linear regression, maize production

1. Introduction

Climate change has been one of the most important global environmental challenges of recent decades, with significant environmental, economic, and social impacts in complex ways. The exposure of crop production is obvious, but its extent varies depending on the climatic, soil, and hydrological conditions of the region and the crop species.

Maize is known to be a heat- and water-intensive crop. In Hungary, rainfall is the most important meteorological factor determining crop yields. In 2021, and especially in 2022, very severe drought affected most of the country, including the Debrecen area (*Gombos* and *Nagy*, 2022, 2023). Data from a maize yield experiment in Debrecen show a strong positive correlation between the amount of rainfall during the growing season and the average yield (*Nagy*, 2012). According to *Márton* (2004), the relationship is not linear, the optimal amount of rainfall depends on the nutrient supply, and in the wettest years yield depression may occur. According to *Szalóki* (1989), the total water requirement of maize is 420–550 mm measured with lysimeter. The water requirement of the crop is significantly higher than the average rainfall of the growing season, with 100–150 mm in the main production areas, and in some places with 200 mm, with only a smaller water deficit (40–80 mm) in the southwestern part of the Transdanubian region (*Nagy*, 2007). The yield security of maize is improved if the deeper layers of the soil are saturated with water in the preceding winter half-year. This effect has been statistically demonstrated in some production areas (*Nagy*, 2012).

Adequate soil moisture is required for germination and initial development, but the water consumption of the plant is not yet significant. Heavy rainfalls in March and April hamper soil preparation and sowing. This can lead to a delay in sowing, especially on compacted soils. Even during the period of intensive vegetative development, maize is not very sensitive to precipitation deficits (*Cheng et al.*, 2021, *Széles et al.*, 2019). This is indicated by the fact that very dry (essentially rainless) weather in June did not in itself reduce the average yield below the average (*Gombos* and *Nagy*, 2019), however, using machine learning methods to study maize yield and its determinants, it was found that May precipitation is one of the most influential parameters (*Nyéki et al.*, 2021).

Precipitation in July and August is particularly important, as the plant's water requirements are greatest during silking, grain setting, and early crop development (*Antal et al.*, 1992). Other studies have also found these phenophases to be essentially the most sensitive to water deficit, with only minor differences in the delimitation of the period (*Westgate* and *Boyer*, 1986; *Smith et al.*, 2004; *Nielsen et al.*, 2010). Thereafter, the water need of maize gradually decreases. Precipitation after physiological maturation has an adverse effect. In September-October, dry, moderately warm weather is optimal, because it accelerates grain dehydration and drying and, consequently, does not hinder harvesting.

Several studies have demonstrated the yield reducing effects of high temperatures (*Schlenker* and *Roberts*, 2009; *Lobell et al.*, 2013; *Ben-Ari et al.*, 2016; *Carter et al.*, 2016), a phenomenon that is becoming increasingly common in Hungary. Maize is most sensitive to heat stress during the reproductive phenophase, especially during silking The viability of pollen is impaired by temperatures above 35 °C, which is further exacerbated when coupled with low humidity (*Fonseca* and *Westgate*, 2005). A french research has shown that the number of days with maximum temperatures above 32 °C explains the interannual variability of the average yield to a degree essentially equal to that of precipitation (*Hawkins et al.*, 2013). Studies by *Schlenker* and *Roberts* (2009) showed a negative effect of temperatures above 29 °C on US county-level yield averages.

Low temperatures do not usually cause irreversible damage. Frost damage is rare if sowing is timed correctly. Major damage to maize occurs only at -2 to -3 °C (*Dhillon et al.*, 1988). At the beginning of the growing season, it is not uncommon for temperatures to be below or just above the base temperature of maize. At this time, plant development is arrested or very slow. Low mean temperatures in April and May result in a prolongation of the phenophases and ultimately the ripening period (this may be partially compensated by later warm weather). Harvesting is either done at higher grain moisture (high drying costs) or later, when the risk of adverse weather is significantly higher, making the harvesting workflow more difficult and increasing harvest losses.

The global average temperature shows a clear and increasing trend. The most recent 10-year period of 2013–2022 shows an average surface temperature 1.15 °C above the average for the period 1851–1900, with a warming rate of

1.65 °C for land (IPCC, 2023). The global average (land) precipitation has shown a weak upward trend over the 20th century, with large inter-decadal variability. The trend has not been significantly decreasing since 1950 (IPCC, 2007). However, the pattern of changes in precipitation patterns shows a high degree of geographical variability. Some areas have become drier than in the past (Southern Europe, Soutwest USA, Sahel, South Africa), while other areas have shown an increasing trend in precipitation (most of the USA, Northern Europe, Northern Asia, Central Asia) (IPCC, 2007; EEA, 2014; USGCRP, 2017).

The change in the national mean temperature in Hungary over the 120-year period 1901–2020 is 1.2 °C, while over the period 1981–2020 it is 1.7 °C. There has been significant warming in all seasons, with the largest increase in the summer temperatures (OMSZ, 2019a). The spring precipitation is the one that shows a clear change, with a 17% decrease. There are differences in the trend of the annual amount between the different parts of the country. There is a decrease in the western part of the country and a slight increase in most of the Great Hungarian Plain. For the period 1981–2020, an upward trend in annual precipitation can already be observed on a national average (OMSZ, 2019b).

Several studies have been carried out to investigate the climatic changes that have taken place in some municipalities and smaller regions of the country. In Keszthely, the trend of annual precipitation decrease in the period 1871–2014 is not significant (*Kocsis* and *Anda*, 2017). Precipitation decrease trends in the spring (-32 mm/100 year), April (-14 mm/100 year), and October (-24 mm/100 year) were found to be significant. *Füzi* and *Ladányi* (2020) investigated various parameters related to frost in the Sopron region (NW-Hungary). All trends show decreasing number of days with different frost level and increasing duration of frost free periods. These results are in agreement with the general warming tendencies. Another study of *Füzi* and *Ladányi* (2022) dealing with various temperature and precipitation indicators describes an increasing frequency of extreme weather events (especially which are related to heat stress) in the Moson Plain.

The main meteorological features of the period 1901–2010 in Debrecen are summarized by *Juhász et al.* (2018). The analysis of the 110-year trends includes, in addition to the classical annual and seasonal mean temperature and precipitation totals, a number of indicators derived from daily data.

The aim of this research is to analyze the climatic changes that have occurred in one of the most important regions, the Hajdúság maize production region in Hungary, which has excellent soil conditions for this crop. The authors consider it important to include data from the most recent years in the trend analysis, and the processed data series should be sufficiently long.

2. Material and methods

2.1. Study area and data

The majority of the Hajdúság, one of the main maize growing areas in Hungary, is located in Hajdú-Bihar county (Hungary), geographically comprising the Hajdúhát and the southern pasrt of Hajdúság. The dominant soil type of the area is loess chernozem with lime deposits, which is a lowland calcareous loess soil with excellent fertility and water management. The area was climatologically analyzed using homogenized temperature and precipitation data from Debrecen, provided by the Hungarian Meteorological Service. The daily resolution database for the period 1901–2020 is freely available for download on the website of the organization (Meteorological Data Repository, OMSZ):

- daily amount of precipitation,
- daily minimum temperature,
- daily maximum temperature,
- daily mean temperature.

The post-1973 part of the series was included in the analysis, supplemented with data for the years 2021–2022. During this period, measurements were taken at the airport located south of the city (47°30' N, 21°38' E, 107 above sea level) (*Fig. 1*).

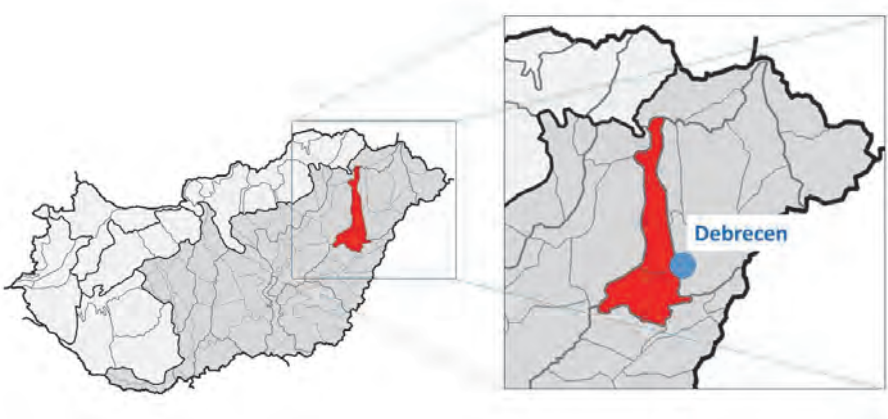

Fig. 1. Geographical position of the study area (Hajdúság area (red), Debrecen-Airport meteorological station)

At the Debrecen-Airport station, the mean annual temperature is 11.0 °C and the mean annual precipitation is 543 mm averaged over the period 1991–2020.

The coldest month is January (-0.8 °C), the warmest is July (21.9 °C). The lowest precipitation is in January-March, the highest in May-July (24 mm in January, 68 mm in July) (*Table 1*).

Table 1. Average monthly temperature and precipitation in Debrecen (1991-2020)

	1	**2**	**3**	**4**	**5**	**6**	**7**	**8**	**9**	**10**	**11**	**12**
T (°C)	-0.8	0.9	5.8	11.9	16.8	20.3	21.9	21.8	16.5	11.0	5.6	0.5
P (mm)	24	32	30	45	59	67	68	46	47	41	41	42

The quality of the database used is fully in line with the research objectives. The data series are homogenized to the current situation, and inhomogeneities due to changes in measurement conditions have been filtered out. In Debrecen, there have been only minor changes in the environment of the measurement site during the 50-year period under study, with one relocation of the station within the airport in 1995. However, the measurement technology changed in 2000 with the automation of the station. The traditional mercury station and maximum and minimum alcohol thermometers have been replaced by a platinum Pt100 resistance thermometer which continuously measures the temperature. A prerequisite for reliable change detection is the use of controlled, homogenized data series. Trend analyses based on raw, non-homogenized data are often misleading and may erroneously detect changes that are the opposite of real changes (*Izsák* and *Szentimrey,* 2020).

2.2. Methods

Trend analysis was used to investigate the climate changes in Debrecen over the past decades until today. Analyses were performed for the last 50-year period (1973–2022) and the last 30-year period (1993–2022). These are long enough periods to identify trends, but do not go back to years irrelevant to current crop production skills. On the basis of the international literature and the authors' own previous research results, the meteorological parameters of importance for maize production were identified and trend analysis was performed on them:

- monthly mean temperatures (April, May, June, July, August, September, October),
- monthly averages of daily minimum temperatures (April, May, June, July, August, September, October),
- monthly averages of daily maximum temperatures (April, May, June, July, August, September, October),

- mean temperatures for winter and summer half-year,
- average daily minimum temperatures in the winter and summer half-year,
- average daily maximum temperatures in the winter and summer half-year,
- annual mean temperature,
- annual average daily minimum temperatures,
- annual average daily maximum temperatures,
- monthly rainfall totals (April, May, June, July, August, September, October),
- total precipitation for the winter half-year (October-March),
- rainfall totals for the summer half-year (April-September),
- annual rainfall amount.

2.3. Trend analysis

Both parametric and non-parametric methods are available for time series trend analysis.

The usual parametric tests require normality and independence of the data. For the non-parametric tests, normality is not a prerequisite, i.e., for many meteorological data sets (e.g., precipitation data or various derived parameters are usually included), the use of the latter is justified. Other arguments in favor of non-parametric methods are that they are less sensitive to outliers and can be applied to both linear and non-linear trends.

The non-parametric Mann-Kendall (rank-based) statistical test (*Mann*, 1945; *Kendall*, 1975) has been widely used in trend analysis of meteorological time series, both for precipitation and temperature (*Wang et al.*, 2013; *Khalili et al.*, 2016; *Skowera et al.*, 2016; *Krebs et al*,. 2021; *Makungo* and *Mashinye*, 2022; *Kubiak-Wójcicka et al.*, 2023). The only prerequisite for this robust method is the independence of data. The associated Sen's slope estimator calculates the slope value (m_{ij}) for each pair of data, and the median of these gives the estimate of the slope (Q) of the linear trend:

$$m_{ij} = (Y - Y_{ji}) / (j-i), \tag{1}$$

$$Q = \text{median}\,(m)_{ij}, \tag{2}$$

where Y_j and Y_i are the values of the meteorological variables at time $t = j$ and $t = i$ ($j > i$), respectively, and i=1, ..., n-1, j=2, ..., n, n is the number of elements in the sample.

The use of linear regression analysis on climate time series is also common in studying trends in terms of temperature and precipitation (*Kocsis* and *Anda*, 2017; *Juhász et al.*, 2018; *Humphries et al.*, 2018; *Karimi et al.*, 2021; *Barna et*

al., 2022). There are several studies where, in addition to linear regression analysis, non-parametric methods are used to investigate climate trends (*Kocsis* and *Anda*, 2018). The equation of the linear regression model is

$$Y = a + b\text{-}X\,, \tag{3}$$

where Y is the dependent variable (e.g., temperature), X is the independent variable (for time series, time, e.g., year), b is the slope of the trend line (e.g., °C/year), and a is the intercept (trend value at time "0").

The coefficients, i.e., the fit of the line, are determined using the least-squares method, which provides the sensitivity of the model to outliers. A positive m value indicates an increasing trend and a negative *m* value indicates a decreasing trend.

As a first step of data processing, an Excel spreadsheet was used to produce the monthly, semi-annual, and annual data series for the period 1973–2022 based on the daily resolution database.

This was followed by a normality test using the SPSS 27 statistical software. For testing normality, the Shapiro-Wilk test was chosen, which is the most recommended and widely used method for small (n<50) samples (*Razali* and *Wah*, 2011; *King* and *Eckersley*, 2019).

Regardless of normality, both parametric and non-parametric trend analyses were performed for each data series. The results were interpreted taking into account the results of the SW test, and if normality was met, the comparison of the two trends provided additional information.

Linear regression calculations with significance testing based on the related two-sided t-test method were also performed using the SPSS 27 statistical software. For the non-parametric procedure, the Excel macro MAKESENS (FMI) developed by the Finnish Meteorological Institute was used. The application determines the significance and slope of the trend based on the Mann-Kendall (MK) test and Sen's slope estimation (*Salmi et al*., 2002). The slope, as the change in trend value per unit time, is presented in units of °C/10 years for temperature values and mm/10 years for precipitation data for ease of interpretation. MAKESENS tests for four levels of significance using the Z-test statistic (α: 0.1, 0.05, 0.01, and 0.001, with two-sided tests). When the aforementioned significance levels are detected, the time series is likely to exhibit a monotonic increasing trend (Z sign positive) or decreasing trend (Z sign negative). Even with α=0.1, there is only a 10% probability of error by rejecting H0 (no trend) (*Salmi et al*, 2002).

2.4. Examination of yields

The performed average yield analyses were based on the results of the maize yield trials conducted at the Debrecen-Látókép experiment site over a 32-year period

from 1991 to 2022. The yield averages of the treatments most representative of farm conditions were included in the analysis.

Trend analysis was performed using the same non-parametric method applied to meteorological data (MAKESENS, *Salmi et al*., 2002). The monthly temperature and precipitation patterns for the 8–8 years falling in the lower and upper quartile were then analyzed based on the yield averages. The comparison of the averages gave an overview of the importance of each monthly meteorological parameter in the evolution of the yield average. A more detailed quantitative analysis of the relationship between the average yield and the weather conditions was not the subject of this research.

3. Results

The normality test on the 50-year data series yielded results in line with the authors' expectations. The normal distribution of the temperature parameters is confirmed in almost all cases by the Shapira-Wilk test with $p > 0.05$ (the only exception is the minimum temperature in October). The monthly precipitation data are not normally distributed, but for longer periods (annual, semi-annual), the test showed normality. Independence is met for all sample elements. Therefore, the performed parametric trend test is relevant for most of the meteorological parameters under study, but should be treated with reservations for monthly precipitation. Non-parametric trend tests do not require a normal distribution, but their use is appropriate in such cases, as they are not sensitive to outliers. In evaluating the changes, the authors relied primarily on the results of the Mann-Kendall test and Sen's slope estimator, which was complemented and compared with the information provided by the parametric method.

3.1. Temperature trends

3.1.1. Monthly temperature

In the period 1973–2022, the monthly mean temperature, the monthly mean of the maximum values, and the monthly mean of the minimum values show an increasing trend in all months considered (*Table 2*). In May and September, the changes are not significant, and the increase is typically only 0.1–0.2 °C/10 years. In April, maximum values increased the most and minimum values the least, and the trend of the mean increase was also close to 0.5 °C/10 years. In the summer months, an upward trend was confirmed for all parameters at the p=0.001 significance level. Maximum temperatures increased most, with a 10-year increase of 0.95 °C in August, and slightly less in June and July (0.78 °C and 0.75 °C, respectively). This is also the order of the months for mean temperatures. The 10-year increases in trend values are 0.73 °C in August, 0.65 °C in June, and 0.56 °C in July. The positive trend for minimum values is 0.5–0.6 °C/10 years for all three summer months. The

warming observed in October is smaller (0.2–0.3 °C/10 years) and shows significance only for the average minimum and maximum values.

Table 2. Trend parameters for monthly temperature data, calculated by non-parametric (Mann-Kendall test and Sen's estimator) and parametric (linear regression) methods. Significance levels are ***: $p<0.001$, **: $p<0.01$, *: $p<0.05$, $^{+}$: $p<0.1$.

Indicator	Month	1973–2022 (50 years) Trend (°C/10 years)^{significance}		1993–2022 (30 years) Trend (°C/10 years)^{significance}	
		MK + Sen's slope	LR	MK + Sen's slope	LR
Average temperature	April	0.46**	0.40***	0.30	0.19
	May	0.11	0.17	-0.44	-0.40
	June	0.65***	0.66***	0.81***	0.80***
	July	0.56***	0.57***	0.63^{+}	0.58***
	August	0.73***	0.68***	0.82*	0.78***
	September	0.14	0.15	0.66^{+}	0.63^{+}
	October	0.20	0.19	0.20	0.23
Minimum temperature	April	0.35*	0.26	0.07	-0.03
	May	0.10	0.13	-0.34	-0.27
	June	0.59***	0.55***	0.73***	0.78***
	July	0.50***	0.51***	0.48^{+}	0.52***
	August	0.55***	0.54***	0.58**	0.61***
	September	0.22	0.19	0.55	0.36
	October	0.26^{+}	0.23	0.20	0.20
Maximum temperature	April	0.74***	0.69***	0.74	0.63
	May	0.28	0.34^{+}	-0.26	-0.25
	June	0.78***	0.79***	0.96**	0.97***
	July	0.75***	0.78***	0.86*	0.77***
	August	0.95***	0.89***	1.00**	1.01***
	September	0.18	0.22	1.07^{+}	0.96^{+}
	October	0.31^{+}	0.35	0.39	0.39

Looking at the 30-year period of 1993–2022, there is a significant difference in May, September, and part of April compared to the previous period. Instead of a slight warming over the 50-year period, the mean temperature in May has decreased by 0.44 °C/10 years (slightly less for the minimum and maximum values) over the last 30 years. Although the change is not significant, it is noteworthy, because this is the only month with a negative temperature trend, and it is also an important month for maize production. In September, instead of the 50-year non-significant positive trend in mean temperature, significant warming (0.66 °C/10 years) is already observed at the p=0.1 level over the last 30 years. The increase in September maximum values is the largest (1.07 °C/10 years). The April mean temperature still shows an upward trend, but it is smaller and no longer significant. The variation in maximum and minimum temperatures is very different. While maximum values show an increasing trend of 0.74 °C/10 years (although not significant), the April mean minimum temperatures show essentially no trend change. For the summer months, the temperature trend over the last 30 years shows a larger 10-year change than over the 50-year period (there was no intense warming in the 70s and 80s). In particular, June and August have seen an increase in temperature, with mean temperatures rising by 0.81 and 0.82 °C/10 years, monthly average minimum values by 0.73 and 0.58 °C/10 years, and maximum values by 0.96 and 1.00°C/10 years.

The trend values obtained by linear regression with least squares fitting for the 50-year data series are in good agreement with the results of the non-parametric trend analysis. In all cases the differences are below 0.1 °C/10 years, but mostly below 0.05 °C/10 years, which is negligible from a practical point of view. For the April minimum values and the October minimum and maximum values, only the MK test showed significance (p=0.05 and p=0.1, respectively). For the May maximum values, the trend was confirmed as significant by the parametric procedure (p=0.1), but not by the MK test. For the 30-year data series, there were differences in the strength of significance. In particular, the significance level of the July and August trends was found to be weaker by the MK test, but there was no significant difference in the magnitude of the increase (< 0.1 °C/10 years).

3.1.2. Annual and semi-annual temperature

The 10-year increase in the annual mean temperature trend over the period 1973–2022 is 0.39 °C. Similar warming (0.41 °C) was observed in the summer half-year, and a slightly smaller warming (0.29 °C) in the winter half-year. The average of the minimum temperatures showed a nearly equal increase on all three time scales (0.33-0.36 °C/10 years). The maximum temperature showed larger warming, with a 10-year trend increase of 0.40 °C in the winter half-year, 0.61 °C in the summer half-year, and 0.52 °C per year (*Table 3*).

The trends over the last 30 years show a more intense warming than that observed in the period 1973–2022, with the exception of the mean summer half-year temperature and the averages of the minimum values. The annual mean temperature is increasing at a rate of 0.52 °C/10 years. The winter half-year mean temperature trend has become about twice as steep (0.62 °C/10 years) as the trend over the 50-year period. The most intense change is detected in the mean maximum temperatures. Here, the trend increases by 0.71 °C, 0.72 °C, and 0.85 °C every 10 years for the annual, summer half-year and winter half-year, periods, respectively.

The rates of change obtained from parametric and non-parametric trend analyses are essentially the same over the 50-year period. Even for the shorter study period, only small differences arise from methodological differences, generally not exceeding 0.05 °C/10 years. For the annual and semi-annual data, all temperature parameters investigated showed a significant trend.

Table 3. Trend parameters for yearly and half-year (h-y) temperature data, calculated by non-parametric (Mann-Kendall test and Sen's estimator) and parametric (linear regression) methods. Significance levels are ***: $p<0.001$, **: $p<0.01$, *: $p<0.05$, $^{+}$: $p<0.1$

Indicator	Time period	1973-2022 (50 years) Trend (°C/10 years)^{significance}		1993-2022 (30 years) Trend (°C/10 years)^{significance}	
		MK + Sen's slope	LR	MK + Sen's slope	LR
Average temperature	Year	0.39***	0.39***	0.52**	0.53***
	Summer h-y	0.41***	0.44***	0.41*	0.43***
	Winter h-y	0.29*	0.33***	0.62*	0.63***
Minimum temperature	Year	0.35***	0.35***	0.52***	0.47***
	Summer h-y	0.36***	0.36***	0.33**	0.33***
	Winter h-y	0.33*	0.33***	0.63*	0.58***
Maximum temperature	Year	0.52***	0.52***	0.71***	0.72***
	Summer h-y	0.61***	0.62***	0.72**	0.69***
	Winter h-y	0.40**	0,41***	0.85*	0.78***

3.2. Precipitation trends

Precipitation shows significantly greater variability than temperature, both on monthly and annual bases. This partly explains why the trends obtained are mostly not significant at the p=0.05 level, or even at the *p*=0.1 level, which provides a wider range (*Table 4*).

Over the longer period, only September showed an increasing (+3.6 mm/10 years) but not significant trend of the examined months. The other months show a non-significant decrease, with October showing the smallest decrease (<1 mm/10 years, practically no change), June the largest (-6.2 mm/10 years), followed by July (-4.5 mm/10 years). The annual precipitation total is also decreasing, with a trend of -17.2 mm/10 years. The decrease has basically taken place in the summer half-year (-15.8 mm/10 years). The trend of 3.2 mm/10 years in the winter is negligible and not significant. The parametric test showed a significant decreasing trend at the p=0.1 level in June (-7.4 mm/10 years) and in the summer half-year values (-15 mm/10 years).

In the period 1993–2022, the two methods show a decreasing precipitation in April (-11.5 mm/half year, p=0.1) in complete agreement. Of the examined months, only October shows an increase in precipitation, but it is not significant and of very small value. From May to September, a slight decrease is observed in all months, but even in May, it is only 4.5 mm/10 years. Decreases in June and July that are more significant in the 50-year base have not been observed for the last 30 years. The trend in precipitation decline in the summer half-year is 27 mm/10 years, while precipitation in the winter half-year hardly changes (+3 mm/10 years is practically negligible). Consistent with these findings, the trend in annual precipitation is also decreasing (non-significant) at a rate of 24 mm/10 years.

Table 4. Trend parameters for monthy, yearly, and half-year (h-y) precipitation data, calculated by non-parametric (Mann-Kendall test and Sen's estimator) and parametric (linear regression) methods. Significance levels are ***: p<0.001, **: p<0.01, *: p<0.05, $^{+}$: p<0.1

Indicator	Time period	1973-2022 (50 years) Trend (mm/10 years)$^{\text{significance}}$		1993-2022 (30 years) Trend (mm/10 years)$^{\text{significance}}$	
		MK + Sen's slope	LR	MK + Sen's slope	LR
Precipitation	April	-2.1	-1.9	-11.5^{+}	-11.6^{+}
	May	-2.0	-3.5	-4.5	-3.6
	June	-6.2	-7.4*	-0.9	-1.4
	July	-4.5	-3.6	-1.7	-3.0
	August	-2.1	-2.7	-2.6	-6.1
	September	3.6	4.0	-0.6	-1.6
	October	-0.8	-1.2	2.3	3.1
	Year	-17.3	-11.6	-24.0	-18.3
	Summer h-y	-15.8	-15.0^{+}	-26.8	-27.2
	Winter h-y	3.2	3.8	3.0	4.9

3.3. Maize yield

In the period 1993–2022, the average yield was 10.4 t/ha in the long-term maize experiment at the Debrecen-Látókép experiment site, under agrotechnologically typical of farm conditions. The value, which is significantly above the national average and the moderate differences between years, is due to the excellent soil conditions (structure, water management properties) (*Fig. 2*). A slightly decreasing but not significant trend can be observed, with a value of 0.20 t/ha.

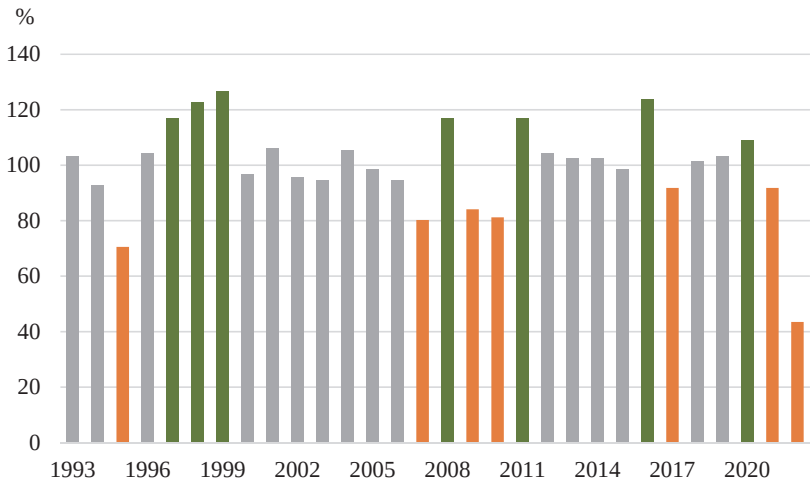

Fig. 2. Annual average yields of the Debrecen-Látókép long-term maize experiments as a percentage of the average yield for the period 1993–2022.

Based on the yield average, weather conditions in the lower and upper quartile years differ most in July. The 8 years with the lowest yields (low yield years) have an average July precipitation of only 36 mm and a mean temperature of 23.1 °C, while the high yield years have average precipitation of 100 mm and 21.3 °C, respectively (*Table 5*). Of the high yield years, there was only one in which the July rainfall total was below the multi-year average, but then the weather was cold, and June and August were both wetter than average.

Table 5. Monthly precipitation sum (ps) and mean temperature (m) values averaged over low yield years (LYY) and high yield years (HYY).

	April	**May**	**June**	**July**	**August**	**September**	**October**
LYY-ps (mm)	38	51	62	36	37	64	43
HYY-ps (mm)	40	63	77	100	50	37	45
LYY-m (°C)	11.2	16.6	21.0	23.1	22.6	16.0	10.5
HYY-m (°C)	11.4	15.8	20.3	21.3	21.1	17.2	10.4

The months of May, June, and August are also shown to be cooler on average and slightly wetter in high yield years. However, these months alone do not tend to have a decisive effect on yields. For example, in half of the low yield years, June was particularly wet.

In April, the average precipitation and temperatures for low and high yield years were almost the same, slightly lower than the 30-year average. The weather in September no longer affects the yield average, as maize has typically reached physiological maturity by this time. However, it is an interesting correlation that, on average over the 8 low yield years, this month is wetter and cooler than the average of the 8 high yield years.

4. Discussion and conclusions

The performed research shows that the trend analysis results and the conclusions that can be drawn from them are influenced by the choice of the length of the study period. The numerical values of the slope of the trend differ, and for some parameters there are also substantial differences (e.g., trend sign), a phenomenon that can be encountered even in the case of the 30- and the 50-year period. Several studies analyze trends of 100 years or more (*Juhász et al.*, 2018; *Kocsis* and *Anda*, 2017), with which comparisons of trends over shorter periods should be treated with caution. The results of the parametric and non-parametric trend analyses for the temperature variables that were included differed only marginally (the choice of period has a much more pronounced effect). There were also only few cases of substantial differences for precipitation data that do not follow a normal distribution (e.g., monthly). In the study by *Kocsis* and *Anda* (2018), the results obtained with the non-parametric method showed better agreement with the results from other studies.

The annual mean temperature increase trends of 0.39 and 0.52 °C/10 years show an increase of around 2 °C over 50 years and 1.5 °C over 30 years, in line with the national average increase over the 1981–2020 period (OMSZ, 2019a).

Juhász et al. (2018) show a warming of 1.4 °C for Debrecen over the 1971–2010 period, but this does not include the most recent warmest years.

There is a significant warming in both the summer and winter half-years, with the summer half-year showing a steeper upward trend in the 50-year series and the winter half-year in the 30-year series. No seasonal analysis clearly comparable to the literature sources has been carried out, but the data clearly show a high, highly significant warming in the summer months and less intense changes in the 2 spring and 2 autumn months. On average in Hungary, the transitional seasons also showed less warming, with winter and summer showing greater warming (OMSZ, 2019a).

The annual and semi-annual maximum values showed a larger increase than the minimum values. The larger daily temperature variation may be related to stronger radiation effects. No studies have been carried out in this respect, but there has been a significant increase in the domestic solar irradiance values (about 200 hours) for the period 1991–2020 compared to the period 1971–2000.

The challenge in analyzing precipitation data series is the high variability that masks trends. Significant trends (p=0.05) are not typically found in monthly or even semi-annual or annual data. No significant change was detected in any of the 50-year data series by the Mann-Kendall test. Only the 30-year April data series showed a trend-like change at the p=0.1 significance level. Nevertheless, the analysis of change provides useful information.

There is a negative, non-significant trend in annual precipitation. The decreases of 17 mm and 24 mm/10 years obtained for the 50- and 30-year time series, respectively, are not negligible from a practical point of view. Previous declining trends in precipitation have been described by other sources (*Szalai*, 2011). Climate change scenarios, with greater uncertainty, have also suggested a continuation of this trend (*Bartholy et al.*, 2011). In contrast, a significant increase is already observed on a national average over the period 1981–2020 (OMSZ, 2019b). Looking at the annual data series separately for the same period in this research, it was found that there is no change in Debrecen, with a non-significant trend of 2.2 mm/10 year decrease.

In the summer half-year, precipitation is decreasing, with a slope of -27 mm/10 years for the last 30 years, but even this is not significant due to its high variability. There is no significant change in the amount of precipitation in the winter half-year over the last decades.

Altogether, the changes are negative for maize production. The clear annual warming tends to increase evaporation, which is accompanied by a slight decrease in precipitation. The two phenomena together lead to a deterioration in the water availability of the crop, which is a key factor for the yield. There are two viewpoints for the decreasing precipitation in April in terms of crop production. On the one hand, it is favorable for seedbed preparation and sowing. On the other hand, especially on soils with more extreme water management (clay, sand), post-sowing rainfall may be necessary for proper emergence. The analysis of the yield

data series also points to this duality. A drier than average April can lead to low or high average yields. Temperatures in April-May have not increased compared to the previous period, i.e., no faster initial development should be expected. In recent years, it has been repeatedly observed that the plant develops slowly and is more exposed to various pests, especially animal pests, during this period. The high yield averages tend to occur in years when the summer months (July in particular) are cooler and wetter than usual. This tendency suggests a markedly unfavorable warming trend in the summer months, which is more pronounced for maximum temperatures. Precipitation also tends to show a downward trend, which is clearly unfavorable. The risk of soil and atmospheric droughts is increasing, especially during the wider interval of the silking-yield formation period, which is critical for maize. Although maize is a heat-sensitive crop, the statement (*Varga-Haszonits* and *Varga*, 2004) that the warmer summer areas of the country are the most favourable from a temperature point of view is no longer true. Rather, the negative impact of heat stress due to excessively high daytime temperatures is becoming a more important factor from a practical aspect. The weather in September and October has become slightly more favorable for the final stages of ripening, watering, drying, and harvesting.

Precision maize farming offers the possibility to at least partially compensate for negative changes by using modern techniques and agrotechnical elements adapted to the changed climatic conditions. Based on the obtained results, the following can be proposed:

- the use of water conservation techniques in soil and seedbed preparation due to lower rainfall in April;
- choosing the appropriate sowing date earlier than usual for a more secure emergence;
- cultivation of a genotype with relatively rapid initial development even at lower temperatures;
- emphasis on agrotechnical methods to reduce the stress and impact of summer water stress.

Acknowledgments: Project no. TKP2021-NKTA-32 has been implemented with the support provided from the National Research, Development and Innovation Fund of Hungary, financed under the TKP2021-NKTA funding scheme.

References

Antal, J., Kismányoky, T., and *Ragasits, I.,* (eds.), 1992: Szántóföldi növénytermesztés. Mezőgazda Kiadó, Budapest. (in Hungarian)

Barna, Zs., Izsák, B., and *Pieczka, I.*, 2022: Trendvizsgálat: óraértékek hazai hőmérsékleti trendje. *Légkör 67*, 122–129. (in Hungarian) https://doi.org/10.56474/legkor.2022.3.1

Bartholy, J., Bozó, L., and *Haszpra, L.*, (Ed.), 2011: Klímaváltozás – 2011. Klímaszcenáriók a Kárpát-medence térségére. Budapest. (in Hungarian)

Ben-Ari, T., Adrian, J., Klein, T., Calanca, P., Van der Velde, M., and *Makowski, D.*, 2016: Identifying indicators for extreme wheat and maize yield losses. *Agric. Forest Meteorol. 220*, 130–140. https://doi.org/10.1016/j.agrformet.2016.01.009

Carter, E.K., Melkonian, J., Riha, S.J., and *Shaw, S.B.*, 2016: Separating heat stress from moisture stress: analyzing yield response to high temperature in irrigated maize. *Environ. Res. Lett. 11*, 094012. http://dx.doi.org/10.1088/1748-9326/11/9/094012

Cheng, M., Wang, H., Fan, J., Zhang, F., and *Wang, X.*, 2021: Effects of Soil Water Deficit at Different Growth Stages on Maize Growth, Yield, and Water Use Efficiency under Alternate Partial Root-Zone Irrigation. *Water 13(2)*, 148. https://doi.org/10.3390/w13020148

Dhillon, D.S., Sharma, R.K., Malbotra, V.V., and *Khehra, A.S.*: 1988. Evaluation of maize germplasm for tolerance to low temperature stress under field and laboratory conditions. *J. Agronomy Crop Sci. 160*, 89–93. http://dx.doi.org/10.1111/j.1439-037X.1988.tb00300.x

EEA, European Environment Agency, 2014. Trends in annual precipitation across Europe. www.eea.europa.eu/data-and-maps/figures/observed-changes-in-annual-precipitation-1961-6

Fonseca, A.E. and *Westgate, M.E.*, 2005: Relationship between dessication and viability of maize pollen. *Field Crops Res. 94*, 114–125. http://dx.doi.org/10.1016/j.fcr.2004.12.001

Füzi, T. and *Ladányi, M.*, 2020: Frost risk indicator analysis in Sopron wine region (1961–2016). *Időjárás 124*, 447–462. https://doi.org/10.28974/idojaras.2020.4.2

Füzi T. and *Ladányi M.*, 2022: Frequency and variability trends of extreme meteorological events in the Moson Plain, Hungary (1961–2018). *Időjárás 126*, 319–334. http://doi.org/10.28974/idojaras.2022.3.3

Gombos, B. and *Nagy, J.*, 2019: Az időjárás értékelése kukorica (Zea mays L.) tartamkísérletek eredményei alapján. *Növénytermelés 69 (2)*, 5–23. (in Hungarian)

Gombos, B. and *Nagy, J.*, 2022: A látóképi kukorica tartamkísérlet 2021-es tenyészidőszakának agrometeorológiai jellemzőinek elemzése. *Növénytermelés 71 (1)*, 7–20. (in Hungarian)

Gombos, B. and *Nagy, J.*, 2023: A 2022-es rendkívüli aszály agrometeorológiai jellemzői Debrecen-Látóképen. *Növénytermelés 72 (1)*, 1–14. (in Hungarian)

Hawkins, E., Fricker, T.E., Challinor, A.J., Ferro, C.A., Ho, C.K., and *Osborne, T.M.*, 2013: Increasing influence of heat stress on French maize yields from the 1960s to the 2030s. *Glob. Change Biol. 19*, 937–947. https://doi.org/10.1111/gcb.12069

OMSZ, Hungarian Meteorological Service, 2019a: Magyarország hőmérsékleti viszonyai. (in Hungarian) https://www.met.hu/eghajlat/magyarorszag_eghajlata/altalanos_eghajlati_jellemzes/homerseklet/

OMSZ, Hungarian Meteorological Service, 2019b: Magyarország csapadék viszonyai. (in Hungarian) https://www.met.hu/eghajlat/magyarorszag_eghajlata/altalanos_eghajlati_jellemzes/csapadek/

Humphries, U., Kaewmesri, P., and *Varnakovida, P.*, 2018: Rainfall trend by linear regression analysis over Indochina Peninsula during 1981-2017 (37 Years). *Int. J. GEOMATE 15 (52)*, 206–213. http://dx.doi.org/10.21660/2018.52.66452

IPCC, 2007: Climate Change 2007: Synthesis Report. Contribution of Working Groups I, II and III to the Fourth Assessment Report of the Intergovernmental Panel on Climate Change (eds. *Core Writing Team, Pachauri, R.K* and *Reisinger*, A.). IPCC, Geneva, Switzerland.

IPCC, 2023: Climate Change 2023: Synthesis Report. A Report of the Intergovernmental Panel on Climate Change. Contribution of Working Groups I, II and III to the Sixth Assessment Report of the Intergovernmental Panel on Climate Change (eds. *Core Writing Team, H. Lee* and *J. Romero*). IPCC, Geneva, Switzerland, (in press)

Izsák, B. and *Szentimrey, T.*, 2020: To what extent does the detection of climate change in Hungary depend on the choice of statistical methods? *Int J Geomath. 11*, 17. https://doi.org/10.1007/s13137-020-00154-y

Juhász Cs., Gálya B., and *Huzsvai L.*, 2018: A klímaváltozás hatása a szárazgazdálkodási rendszerekre. Debreceni Egyetem MÉK. (in Hungarian)

Karimi, S., Nazaripour, H. and *Hamidianpour, M.*, 2021: Spatial and temporal variability of precipitation extreme indices in arid and semi-arid regions of Iran for the last half-century. *Időjárás 125*, 83–104. http://dx.doi.org/10.28974/idojaras.2021.1.4

Kendall, M.G., 1975: Rank correlation methods. Charles Griffin, London.
Khalili, K., Tahoudi, M.N., Mirabbasi, R., and *Ahmadi, F.*, 2016: Investigation of spatial and temporal variability of precipitation in Iran over the last half century. *Stoch. Environ. Res. Risk Assess. 30*, 1205–1221. https://doi.org/10.1007/s00477-015-1095-4
King, A.P. and *Eckersley, R.J.*, 2019: Chapter 7 - Inferential Statistics IV: Choosing a Hypothesis Test. *Stat. Biomed. Engin. Sci.* 147-171. https://doi.org/10.1016/B978-0-08-102939-8.00016-5
Kocsis, T. and *Anda, A.*, 2017: Analysis of precipitation time series at Keszthely, Hungary (1871–2014). *Időjárás 121*, 63–78.
Kocsis, T. and *Anda, A.*, 2018: Parametric or non-parametric: analysis of rainfall time series at a Hungarian meteorological station. *Időjárás 122*, 203–216.
Krebs, G., Camhy, D., and *Muschalla, D.*, 2021: Hydro-Meteorological Trends in an Austrian Low-Mountain Catchment. *Climate 9 (8)*, 122. https://doi.org/10.3390/cli9080122
Kubiak-Wójcicka, K., Nagy, P., Pilarska, A., and *Zeleňáková, M.*, 2023: Trend Analysis of Selected Hydroclimatic Variables for the Hornad Catchment (Slovakia). *Water 15 (3)*, 471. https://doi.org/10.3390/w15030471
Lobell, D.B., Hammer, G.L., McLean, G., Messina, C., Roberts, M.J., and *Schlenker, W.*, 2013: The critical role of extreme heat for maize production in the United States. *Nat. Clim. Change 33*, 497–501. http://dx.doi.org/10.1038/nclimate1832
Makungo, R. and *Mashinye, M.D.*, 2022: Long-term trends and changes in rainfall magnitude and duration in a semi-arid catchment, South Africa. *J. Water Climate Change 13*, 2319–2336. https://doi.org/10.2166/wcc.2022.427
Mann, H.B., 1945: Nonparametric tests against trend. Econometrica 13, 245–259. https://doi.org/10.2307/1907187
Márton L., 2004: A műtrágyázás és a csapadék változékonyságának hatása a kukorica (Zea mays L.) termésére. *Agrokémia és talajtan 5*, 309–324. (in Hungarian) https://doi.org/10.1556/Agrokem.54.2005.3-4.5
Nagy J., 2007: Kukoricatermesztés. Akadémiai Kiadó, Budapest. (in Hungarian)
Nagy J., 2012: The effect of fertilization and precipitation on the yield of maize (Zea mays L.) in a long-term experiment. *Időjárás 116*, 39–52.
Nielsen, D.C., Halvorson, A.D., and *Vigil, M.F.*, 2010: Critical precipitation period for dryland maize production. *Field Crops Res. 118*, 259–263. https://doi.org/10.1016/j.fcr.2010.06.004
Nyéki, A., Kerepesi, Cs., Daróczy, B., Benczúr A., Milics, G., Nagy, J., Harsányi, E., Kovács, A.J., and *Neményi, M.*, 2021: Application of spatio-temporal data in site-specific maize yield prediction with machine learning methods. *Prec. Agric. 22*, 1397–1415. https://doi.org/10.1007/s11119-021-09833-8
Razali, N.M. and *Wah, Y.B.*, 2011: Power comparisons of Shapiro-Wilk, Kolmogorov-Smirnov, Lilliefors and Anderson-Darling tests. *J. Stat. Model. Anal. 2*, 21–33.
Salmi, T., Maatta, A., Anttila, P., Ruoho-Airola, T., and *Amnell, T.*, 2002: Detecting trends of annual values of atmospheric pollutants by the Mann–Kendall test and Sen's slope estimates—the Excel template application MAKESENS. Finnish Meteorological Institute, Helsinki.
Schlenker, W. and *Roberts, M.J.*, 2009: Nonlinear temperature effects indicate severe damages to US crop yields under climate change. *Proc. Natl. Acad. Sci. 106*, 15594–15598. https://doi.org/10.1073/pnas.0906865106
Skowera, B., Kopcinska, J., and *Bokwa, A.*, 2016: Changes in the structure of days with precipitation in Southern Poland in 1971–2010. *Időjárás 120*, 365–381.
Smith, W.C., Betran, J., and *Runge, E.C.A.* (eds), 2004: Corn. Origin, History, Technology, and Production. Hoboken, NJ: John Wiley.
Szalai, S., 2011: Magyarország hidroklimatológiai jellemzése. *KLÍMA-21 Füzetek 65*, 17–28. (in Hungarian)
Szalóki, S., 1989: A növények vízigénye, vízhasznosítása és öntözővíz-szükséglete. In (Ed. *Szalai Gy*.) Az öntözés gyakorlati kézikönyve. Mezőgazda Kiadó, Budapest. 100–154. (in Hungarian)
Széles, A., Kovács, K., and *Ferencsik, S.*, 2019: The effect of crop years and nitrogen basal and top dressing on the yield of different maize genotypes and marginal revenue. *Időjárás 123*, 265–278.

USGCRP, 2017: Climate Science Special Report: Fourth National Climate Assessment, Volume I (eds. *Wuebbles, D.J., Fahey, D.W., Hibbard, K.A., Dokken, D.J., Stewart, B.C.,* and *Maycock, T.K.*). U.S. Global Change Research Program, Washington, DC, USA. http://doi.org...7930/J0J964J6

Varga-Haszonits, Z. and *Varga, Z.*, 2004: A meteorológiai viszonyok hatása a kukorica életjelenségeire. II. Agroinform Kiadó, Budapest, *Növényvédelmi tanácsok 13*, 14–16. (in Hungarian)

Wang, S., Zhang, X., Liu, Z., and *Wang, D.*, 2013: Trend Analysis of Precipitation in the Jinsha River Basin in China. *J. Hydrometeorol. 14*, 290–303. https://doi.org/10.1175/JHM-D-12-033.1

Westgate, M.E. and *Boyer, J.S.*, 1986: Reproduction at low silk and pollen water potentials in maize. *Crop Science 26*, 951–956.

IDŐJÁRÁS

VOLUME 127 * 2023

BUDAPEST, HUNGARY

AUTHOR INDEX

TABLE OF CONTENTS

I. papers

SUBJECT INDEX

V

W

Z

INSTRUCTIONS TO AUTHORS OF *IDŐJÁRÁS*

The purpose of the journal is to publish papers in any field of meteorology and atmosphere related scientific areas. These may be

- research papers on new results of scientific investigations,
- critical review articles summarizing the current state of art of a certain topic,
- short contributions dealing with a particular question.

Some issues contain "News" and "Book review", therefore, such contributions are also welcome. The papers must be in American English and should be checked by a native speaker if necessary.

Authors are requested to send their manuscripts to

Editor-in Chief of IDŐJÁRÁS
P.O. Box 38, H-1525 Budapest, Hungary
E-mail: journal.idojaras@met.hu

including all illustrations. MS Word format is preferred in electronic submission. Papers will then be reviewed normally by two independent referees, who remain unidentified for the author(s). The Editor-in-Chief will inform the author(s) whether or not the paper is acceptable for publication, and what modifications, if any, are necessary.

Please, follow the order given below when typing manuscripts.

Title page should consist of the title, the name(s) of the author(s), their affiliation(s) including full postal and e-mail address(es). In case of more than one author, the corresponding author must be identified.

Abstract: should contain the purpose, the applied data and methods as well as the basic conclusion(s) of the paper.

Key-words: must be included (from 5 to 10) to help to classify the topic.

Text: has to be typed in single spacing on an A4 size paper using 14 pt Times New Roman font if possible. Use of S.I. units are expected, and the use of negative exponent is preferred to fractional sign. Mathematical formulae are expected to be as simple as possible and numbered in parentheses at the right margin.

All publications cited in the text should be presented in the *list of references*, arranged in alphabetical order. For an article: name(s) of author(s) in Italics, year, title of article, name of journal, volume, number (the latter two in Italics) and pages. E.g., *Nathan, K.K.,* 1986: A note on the relationship between photosynthetically active radiation and cloud amount. *Időjárás 90,* 10–13. For a book: name(s) of author(s), year, title of the book (all in Italics except the year), publisher and place of publication. E.g., *Junge, C.E.*, 1963: *Air Chemistry and Radioactivity.* Academic Press, New York and London. Reference in the text should contain the name(s) of the author(s) in Italics and year of publication. E.g., in the case of one author: *Miller* (1989); in the case of two authors: *Gamov* and *Cleveland* (1973); and if there are more than two authors: *Smith et al.* (1990). If the name of the author cannot be fitted into the text: *(Miller,* 1989); etc. When referring papers published in the same year by the same author, letters a, b, c, etc. should follow the year of publication. DOI numbers of references should be provided if applicable.

Tables should be marked by Arabic numbers and printed in separate sheets with their numbers and legends given below them. Avoid too lengthy or complicated tables, or tables duplicating results given in other form in the manuscript (e.g., graphs). *Figures* should also be marked with Arabic numbers and printed in black and white or color (under special arrangement) in separate sheets with their numbers and captions given below them. JPG, TIF, GIF, BMP or PNG formats should be used for electronic artwork submission.

More information for authors is available: journal.idojaras@met.hu

Published by the Hungarian Meteorological Service

Budapest, Hungary

ISSN 0324-6329 (Print)

ISSN 2677-187X (Online)